Monthly Notices of the ROYAL ASTRONOMICAL SOCIETY

MNRAS **544,** 1843–1860 (2025) https://doi.org/10.1093/mnras/staf1827
Advance Access publication 2025 October 22

Discovery of 30 Galactic radio transient pulsars with MeerTRAP

J. Tian [1]★ S. Singh,[1]★ B. W. Stappers [1] J. D. Turner [1] K. M. Rajwade,[2] M. C. Bezuidenhout [3,4] M. Caleb,[5,6] I. Pastor-Marazuela [1,7] F. Jankowski [8] V. Gupta,[9] C. Flynn,[9] R. Karuppusamy,[10] E. D. Barr,[10] M. Kramer,[10] R. Breton [1] C. J. Clark [11,12] D. J. Champion [10] and T. Thongmeearkom [1,13]

[1]*Jodrell Bank Centre for Astrophysics, Department of Physics and Astronomy, The University of Manchester, Manchester M13 9PL, UK*
[2]*Astrophysics, The University of Oxford, Denys Wilkinson Building, Keble Road, Oxford OX1 3RH, UK*
[3]*Centre for Space Research, North-West University, Potchefstroom 2531, South Africa*
[4]*Department of Mathematical Sciences, University of South Africa, Cnr Christiaan de Wet Rd and Pioneer Avenue, Florida Park, Roodepoort 1709, South Africa*
[5]*Sydney Institute for Astronomy, School of Physics, The University of Sydney, NSW 2006, Australia*
[6]*ARC Centre of Excellence for Gravitational Wave Discovery (OzGrav), Hawthorn, VIC 3122, Australia*
[7]*ASTRON, the Netherlands Institute for Radio Astronomy, Oude Hoogeveensedijk 4, NL-7991 PD Dwingeloo, the Netherlands*
[8]*LPC2E, OSUC, Univ Orleans, CNRS, CNES, Observatoire de Paris, F-45071 Orleans, France*
[9]*Centre for Astrophysics and Supercomputing, Swinburne University of Technology, Mail H30, PO Box 218, Hawthorn, VIC 3122, Australia*
[10]*Max-Planck-Institut fur Radioastronomie, D-53121 Bonn, Germany*
[11]*Max Planck Institute for Gravitational Physics (Albert Einstein Institute), D-30167 Hannover, Germany*
[12]*Leibniz Universität Hannover, D-30167 Hannover, Germany*
[13]*National Astronomical Research Institute of Thailand, Don Kaeo, Mae Rim, Chiang Mai 50180, Thailand*

Accepted 2025 October 20. Received 2025 October 3; in original form 2025 August 6

ABSTRACT

We present the discovery of 30 new Galactic sources from the MeerTRAP project, a commensal fast radio transient search programme using the MeerKAT telescope. These sources were all identified via a single-pulse search. Most of them are likely to be rotating radio transients given their low pulse rates. Using data captured in our transient buffer, we have localized nine sources in the image domain to arcsecond precision. This facilitates the timing of these sources and further follow-up with other telescopes. Using the arrival times of single pulses, we have constrained the periods of 14 sources, ranging from 121 ms to 7.623 s, and derived a phase-coherent timing solution for one of them. Follow-up observations of the MeerTRAP sources (including those published previously) performed with the Effelsberg telescope have detected regular but faint emission from three sources, confirming their long rotation period, including PSR J2218+2902 with a period of 17.5 s, the fourth slowest in the radio pulsar population. A few of the sources exhibit interesting emission features, such as periodic microstructure in PSR J1243−0435 and possible nulling in PSR J1911−2020 and PSR J1243−0435. We find that the duty cycles of the three newly discovered pulsars are very low and follow the general trend for the duty cycle with period of known pulsars.

Key words: stars: neutron – pulsars: general – radio continuum: transients.

1 INTRODUCTION

Fast radio transients are short-duration radio signals of astrophysical origin (J. M. Cordes & M. A. McLaughlin 2003). Such short time-scale signals are thought to be associated with extreme and dynamic astrophysical phenomena because of the rapid release of immense amounts of energy from a small region (J.-P. Macquart et al. 2010). The fast radio transients of extragalactic origin are known as fast radio bursts (FRBs; see D. R. Lorimer, M. A. McLaughlin & M. Bailes 2024 for an overview). The origin of FRBs is still unknown (E. Platts et al. 2019; B. Zhang 2023). The Galactic fast radio transients are thought to mostly originate from highly magnetized and rotating neutron stars. This includes pulsars (e.g. V. S. Beskin et al. 2015), magnetars (e.g. S. Mereghetti, J. A. Pons & A. Melatos 2015), and rotating radio transients (RRATs; M. A. McLaughlin et al. 2006; E. F. Keane & M. A. McLaughlin 2011).

RRATs are Galactic radio transients with an underlying periodicity similar to that of pulsars, but have low pulse rates (E. F. Keane & M. A. McLaughlin 2011). Their low pulse rates make it difficult to find them in regular pulsar surveys with a periodicity search (M. A. McLaughlin & J. M. Cordes 2003; E. F. Keane & M. A. McLaughlin 2011). While some RRATs have long periods and high magnetic fields, similar to magnetars (A. G. Lyne et al. 2009; M. A. McLaughlin et al. 2009), others show emission properties similar to radio pulsars. M. Caleb et al. (2019) show that the folded profiles of RRATs are highly linearly polarized (∼40 per cent on average),

★ E-mail: jun.tian@manchester.ac.uk (JT); shubham.singh@manchester.ac.uk (SS)

while their individual pulses can be up to ∼100 per cent linearly polarized. RRAT J0139+3336 has recently been shown to follow the rotating vector model usually seen in pulsars (S. J. Dang et al. 2024). Similarly, RRAT J1854+0306 was seen in two different emission modes at two different observing epochs (J. Lu et al. 2019). Microstructure has been seen in at least two RRATs (J0139+3339 and J1918−0449) with the Five-hundred-meter Aperture Spherical Telescope (FAST; J. L. Chen et al. 2022; S. J. Dang et al. 2024). These observed features resemble those seen in pulsar radio emission. Therefore, studying RRATs will help us understand the link between RRATs and normal pulsars.

Magnetars are another class of Galactic transients discovered through their high-energy transient behaviour, but a subclass of these sources show radio emission as well (see S. Mereghetti et al. 2015 and V. M. Kaspi & A. M. Beloborodov 2017 for an overview). RRATs and radio-loud magnetars have some common properties, such as their sporadic radio emission and similar pulse morphology, including microstructure (M. Kramer et al. 2024). Moreover, it has been proposed that some RRATs could be associated with X-ray outbursts of magnetars (e.g. N. Rea et al. 2009; R. F. Archibald et al. 2017), which is supported by the similar spin-down properties of RRATs and magnetars as well as their typically strong magnetic fields (up to 5×10^{13} G; A. G. Lyne et al. 2009; M. A. McLaughlin et al. 2009).

There is evidence of a connection between FRBs and magnetars. An FRB-like signal from the Galactic magnetar SGR 1935+2154 (C. D. Bochenek et al. 2020; CHIME/FRB Collaboration 2020) suggests that at least some FRBs could arise from magnetars. This emission also has luminosity comparable to the faintest and nearest extragalactic FRBs (C. Patel et al. 2018; CHIME/FRB Collaboration 2019). In addition, a few FRBs show pulsar-like polarization position angle swings that are in agreement with the rotating vector model (X. Liu et al. 2025; R. Mckinven et al. 2025), and a few other FRBs show quasi-periodic substructure (W. A. Majid et al. 2021; CHIME Collaboration 2022; I. Pastor-Marazuela et al. 2023). Given these observational similarities between RRATs, magnetars, and FRBs, finding and studying more Galactic transients is crucial to advance our understanding of their connection.

The slow-rotating neutron star population is becoming increasingly interesting with new discoveries of long-period (period of a few tens of seconds; e.g. C. M. Tan et al. 2018; V. Morello et al. 2020a; M. Caleb et al. 2022; Y. Wang et al. 2025) and ultra-long-period (ULP; period of a few minute time-scales; e.g. N. Hurley-Walker et al. 2023, 2024) sources. Not all of them may be neutron stars, and some ULPs are likely to be white dwarf binaries, e.g. GLEAM-X J0704−37 (N. Hurley-Walker et al. 2024) and ILT J1101+5521 (I. Ruiter et al. 2025). If some of these sources are indeed neutron stars, it will challenge the conventional understanding of radio emission from neutron stars (M. Caleb et al. 2022). There is also tentative evidence suggesting that long-period radio sources could be radio-loud magnetars (M. Caleb et al. 2022; M. P. Surnis et al. 2023; Y. W. J. Lee et al. 2025). There are only half a dozen sources with periods between a few tens of seconds and a few minutes (C. M. Tan et al. 2018; V. Morello et al. 2020a; M. Caleb et al. 2022; M. P. Surnis et al. 2023; F. A. Dong et al. 2025b; Y. Wang et al. 2025). Galactic transients like RRATs and magnetars are mostly long-period sources. Discovery and characterization of new Galactic transients can add more sources to the slow-rotating neutron star population or reveal different source populations.

There are two commonly used methods to search for short-time-scale radio signals: periodicity searches and single-pulse searches. Fast transients such as FRBs that do not have any strict periodicity can only be discovered by a single-pulse search (K. M. Rajwade & J. van Leeuwen 2024). Transients with an underlying periodicity can be discovered by periodicity search methods (D. H. Staelin 1969; S. M. Ransom, S. S. Eikenberry & J. Middleditch 2002; V. Morello et al. 2020b). Even when Galactic transients like RRATs do have underlying periodicity, they are usually discovered in single-pulse searches due to their sporadic emission (M. A. McLaughlin & J. M. Cordes 2003; E. F. Keane & M. A. McLaughlin 2011). Some RRATs also show pulsar-like, faint emission (e.g. J. Zhang et al. 2024; S. J. Mcsweeney et al. 2025), which could be detected via a periodicity search.

There have been many single-pulse searches for Galactic transient sources, e.g. realfast at the Jansky Very Large Array (C. J. Law et al. 2018), CRACO at the Australian Square Kilometre Array Pathfinder (Z. Wang et al. 2025b), GHRSS and SPOTLIGHT at the Giant Metrewave Radio Telescope (B. Bhattacharyya et al. 2019; U. Panda et al. 2024), HTRU-South at the Murriyang telescope (M. J. Keith et al. 2010), HTRU-North at the Effelsberg telescope (E. D. Barr et al. 2013), and SMIRF at the UTMOST telescope (V. Venkatraman Krishnan et al. 2020). D. C. Good et al. (2021) discovered seven new Galactic sources with the Canadian Hydrogen Intensity Mapping Experiment (CHIME)/FRB (CHIME/FRB Collaboration 2018), of which four appear to be RRATs and the others intermittent or nulling pulsars, which display intermittent emission but behave like normal pulsars when active. This is followed by another set of discoveries by CHIME/FRB using the same method, which includes 14 RRATs and seven pulsars (F. A. Dong et al. 2023). The FAST Galactic Plane Pulsar Snapshot survey, in addition to a traditional periodicity search, has also performed a single-pulse search and discovered 76 new transient radio sources (D. J. Zhou et al. 2023).

We have been using the Meer(more) TRAnsients and Pulsars (MeerTRAP; S. Sanidas et al. 2018; M. C. Bezuidenhout et al. 2022; K. M. Rajwade et al. 2022; M. Caleb et al. 2023; F. Jankowski et al. 2023; L. N. Driessen et al. 2024) project to perform commensal, time-domain searches for fast transients in real-time with the MeerKAT telescope in South Africa. Thanks to the wide field of view and high sensitivity of MeerKAT, this search program has discovered a few dozen Galactic radio transients (M. C. Bezuidenhout et al. 2022; J. D. Turner et al. 2025). M. C. Bezuidenhout et al. (2022) presented the first discovery of 12 Galactic sources by MeerTRAP, followed by the report of another 26 new sources by J. D. Turner et al. (2025). In this paper, we present 30 more MeerTRAP Galactic sources. In Section 2, we briefly summarize the observational configuration of MeerKAT and the real-time search pipeline, and describe the offline data processing. We also introduce follow-up observations, including sources previously discovered. Our results are then presented in Section 3. We discuss some interesting sources and future prospects in Section 4, followed by conclusions in Section 5.

2 OBSERVATIONS AND DATA REDUCTION

2.1 MeerKAT data processing

2.1.1 Array configuration and data recording

MeerTRAP is a commensal project that piggybacks on other science observations to search for fast transients (B. Stappers 2018; M. C. Bezuidenhout et al. 2022; J. D. Turner et al. 2025). The sky coverage depends on the targets of these surveys, and the observing frequency band is determined by the MeerKAT receivers being used during these observations (M. C. Bezuidenhout et al. 2022). The sources reported in this paper were discovered either in the

UHF (544–1088 MHz; R. Lehmensiek & I. P. Theron 2014) or L (856–1712 MHz; R. Lehmensiek & I. P. Theron 2012) bands. The time-domain data are recorded simultaneously with coherent and incoherent beam modes. The incoherent beam uses all the working antennas available at the time of observation, which can be up to 64. The MeerKAT incoherent beam has a very wide field of view (half power area of 1 deg^2 in the L band and 2.4 deg^2 in the UHF band; T. Mauch et al. 2020). Up to 768 coherent beams are formed to partially cover this field of view. The coherent beams only use the central 40–44 antennas within a baseline of 1 km. These coherent beams are arranged so that they are always between one and five times more sensitive than the incoherent beam (K. M. Rajwade et al. 2022). Data from these beams are recorded at a time resolution of 482 μs in the case of UHF band or 306 μs in the case of L-band observations. The number of frequency channels is 1024 for these observations.

2.1.2 *Real-time pulse searches*

The MeerTRAP search pipeline searches the coherent and incoherent beam data for dispersed single pulses in real time. The data are cleaned for zero dispersion measure (DM) radio frequency interference (RFI; R. P. Eatough, E. F. Keane & A. G. Lyne 2009). Then IQRM cleaning is employed with a threshold of 3σ to filter out narrow-band RFI (V. Morello, K. M. Rajwade & B. W. Stappers 2022). To further reject the zero-DM RFI, all the detections with DM below 20 pc cm^{-3} are rejected. We search up to DM of 2100 pc cm^{-3} in the case of UHF and up to 3600 pc cm^{-3} in the case of L-band observations. The detections above 8σ significance are then sifted and classified using FRBID.[1] See K. M. Rajwade et al. (2022) for a more detailed description of the search pipeline.

2.1.3 *Localization*

Since the coherent beam uses a maximum baseline of 1 km, the discoveries from the time-domain search have moderate uncertainties in their location (∼arcmin). An extra localization effort is needed to increase the accuracy of the source coordinates which can then be used for more sensitive follow-up observation of the source. The coherent beams are arranged to overlap at their 50 per cent sensitivity level. If a source has been detected in three or more coherent beams, it may be localized to the overlapping region of those beams, assuming that the pulse detected by a single tied-array beam of MeerKAT originates within that beam, which is usually the case except for beams lying on the edge of the tiling. This is carried out using the multibeam localization tool SEEKAT[2] (M. C. Bezuidenhout et al. 2023), with the point spread function of each observation being simulated using MOSAIC[3] (W. Chen et al. 2021).

A more accurate localization can be achieved for detections that trigger the transient buffer to store ∼300 ms of voltage data from individual antennas (K. M. Rajwade et al. 2024). The data in the transient buffer are correlated with xGPU[4] (M. A. Clark, P. C. La Plante & L. J. Greenhill 2011) and then converted to measurement sets with DiFX (A. T. Deller et al. 2007, 2011). Then on-pulse and off-pulse images are made with WSCLEAN (A. R. Offringa et al. 2014). The transient buffer stores data from all antennas in the total array, not just those used in beamforming and this can be up to 64 with a maximum baseline of ∼8 km (J. Jonas & MeerKAT Team 2018). The pulse signal-to-noise ratio (S/N) is therefore expected to be higher in these data than in the coherent beams. The on-pulse and off-pulse images are then compared to identify the transient point source. The final position is determined using the Python Blob Detector and Source Finder (PYBDSF),[5] and the absolute astrometry is corrected using catalogued sources from the Rapid ASKAP Continuum Survey (RACS; D. McConnell et al. 2020), as described in L. N. Driessen et al. (2022, 2024). This method usually results in a localization accuracy of ∼1 arcsec, which consists of three components: the source fitting error given by PYBDSF; the systematic uncertainty in the RACS positions; and the median offset of the positions after the astrometric correction. More details about the voltage data reduction and imaging can be found in K. M. Rajwade et al. (2024), J. Tian et al. (2024), and I. Pastor-Marazuela et al. (2025).

2.2 DM determination

For each source presented here, we select the brightest pulse detection to determine the S/N maximizing DM. Then we refined this DM using SCATFIT,[6] which models subbanded pulse profiles with exponentially modified Gaussians that take into account the pulse broadening due to scattering and intrachannel dispersion smearing (F. Jankowski et al. 2023). This method is based on a Bayesian analysis by Markov chain Monte Carlo sampling and provides a refined DM measurement and uncertainty. For some pulses with low S/Ns, we downsampled the data in time by a factor of up to 8, and in frequency to eight subbands, before fitting a scattered pulse model. Subbands with S/N < 3 were not included in the fit. The DM with the lowest Bayesian information criterion (BIC) for each source is listed in Table 2.

2.3 Period search

For some sources that have multiple pulses detected, we calculated the times of arrival (TOAs) of pulses to measure their spin period. We used MAKE_TOAS,[7] an implementation based on MTCUTILS,[8] to calculate the TOA of each single pulse. This was done by convolving single-Gaussian templates with dedispersed time series using SPYDEN.[9] The TOA is given by the peak of the best-matched Gaussian, and its uncertainty is the pulse width divided by the S/N. Under this method, pulses that have more complicated shapes or multiple components will have TOAs that are noisier; however, this noise will always be much smaller than the rotational period.

An initial period estimate is attempted based on the spacing between TOAs measured for a source. We used RRATSOLVE[10] to find the largest period connecting all TOAs. This method requires at least three TOAs closely spaced in time. If a source is detected multiple times over a long time span, we can use the pulsar timing software TEMPO2[11] (G. B. Hobbs, R. T. Edwards & R. N. Manchester 2006) to obtain a phase-connected timing solution. The initial pulsar ephemeris contains the period estimated by RRATSOLVE and the position from the relevant localization technique. Since the timing

[1] https://github.com/Zafiirah13/FRBID
[2] https://github.com/BezuidenhoutMC/SeeKAT
[3] https://github.com/wchenastro/Mosaic
[4] xGPU: https://github.com/GPU-correlators/xGPU
[5] https://www.astron.nl/citt/pybdsf/
[6] https://github.com/fjankowsk/scatfit
[7] https://bitbucket.org/meertrap-ipm/mtcutils/src/jturner-timing/
[8] https://bitbucket.org/vmorello/mtcutils by Vincent Morello, modified by Inès Pastor-Marazuela and James Turner.
[9] https://bitbucket.org/vmorello/spyden
[10] https://github.com/v-morello/rratsolve
[11] https://bitbucket.org/psrsoft/tempo2/src/master/

Table 1. Discovery information for the reported transient sources. We mark the sources independently discovered by other surveys with the asterisk (∗). See Section 3 for more details.

MTP name	PSR J2000 name	Disc. MJD	Disc. project[a]	Disc. mode[b]	Disc. S/N	Disc. DM (pc cm^{-3})	$T_{\rm obs_{IB}}$ [c] (h)	$T_{\rm obs_{CB}}$ [c] (h)	$N_{\rm det}$ [d]	$N_{\rm e}$ [e]	Band[f]
MTP 0051		59627.859034	SCI-20200703-MK-01	IB	8.8	99.16	92.1	0.32	2	2	L
MTP 0052		59622.359342	SCI-20200703-MK-01	CB	8.9	294.41	27.06	0.16	2	1	L
MTP 0053		59637.706047	SCI-20200703-MK-01	CB	9.4	301.47	31.55	0.23	1	1	L
MTP 0054*	J1655−40	59640.062581	SCI-20200703-MK-01	CB	10.6	89.95	48.62	0.16	1	1	L
MTP 0055*	J0917−4420	59636.753994	SCI-20200703-MK-01	CB	12.1	46.36	14.39	1.91	26	8	L, UHF
MTP 0056		59657.066965	SCI-20180516-PW-01	CB	8.2	85.35	56.73	16.99	1	1	L
MTP 0057	J2317−4746	59653.460728	SCI-20180516-NG-02	CB	9.9	23.64	26.33	1.93	6	1	UHF
MTP 0058	J2218−1229	59673.167861	SCI-20180516-NG-02	CB	9.5	29.78	2.86	2.44	6	1	UHF
MTP 0059		59699.528926	SCI-20200703-MK-01	CB	11.9	151.04	34.2	0.23	1	1	L
MTP 0060	J1953−6111	59702.000543	SCI-20180516-EB-01	IB	9.3	41.45	63.17	1	60	5	L
MTP 0061		59707.893381	SCI-20200703-MK-01	CB	12	35.30	42.1	0.16	2	1	L
MTP 0062		59718.143078	SCI-20180516-MB-02	IB	10.6	46.05	70.29	0.73	1	1	L
MTP 0063	J1817−1932	59738.97037	SCI-20180516-PW-01	CB	8.9	217.05	23.66	1.24	128	5	L
MTP 0064		59744.751323	SCI-20180516-NG-02	CB	8.5	65.08	12.37	0.94	1	1	UHF
MTP 0065	J1748−3616	59733.922209	SCI-20180516-PW-01	CB	8.4	268.01	71.44	3.92	9	4	L
MTP 0066		59730.319017	SCI-20180923-MK-02	IB	10.9	149.20	2.23	1.58	2	2	UHF
MTP 0067*	J0933−4604	59782.389429	SCI-20200703-MK-01	CB	11.6	120.34	35.38	0.17	33	2	L
MTP 0068*	J1243−0435	59823.507436	SCI-20180516-NG-02	CB	9.1	21.49	3.9	2.16	5	1	UHF
MTP 0069	J1548−5229	59824.761269	SCI-20180516-MB-02	CB	10.8	366.25	74.8	0.5	3	2	L
MTP 0070*	J1909+0310g	59833.705494	SCI-20180516-MB-02	CB	10.8	110.83	25.8	1.99	1	1	L
MTP 0071		59835.497437	SCI-20200703-MK-02	IB	12.0	98.55	27.14	2.29	1	1	UHF
MTP 0072	J1831−1141	59862.615789	SCI-20180516-MB-02	CB	8.9	40.83	61.25	0.04	4	3	L
MTP 0073		59852.504214	SCI-20180516-PW-01	CB	8.3	304.54	110.97	0.42	1	1	L
MTP 0074*	J1956+3544	59883.607779	SCI-20180516-PW-01	IB	11.4	153.81	1.74	0	16	3	L, UHF
MTP 0075*	J1303−4713	59882.153474	SCI-20180923-MK-02	CB	14.4	82.89	26.88	0.66	3	2	UHF
MTP 0076		59884.557832	SCI-20200703-MK-01	CB	10.1	283.05	30.64	0.34	3	2	L
MTP 0077	J1843−0858	59921.378900	SCI-20180516-MB-02	CB	9.9	300.86	74.79	3.68	11	4	L, UHF
MTP 0078*	J1914+0217	59897.552995	SCI-20180516-MB-02	CB	16.0	161.18	18.92	1.77	12	7	L
MTP 0079	J1816−2419	59964.254553	SSV-20220221-SA-01	CB	10.7	269.24	49.43	9.3	34	6	L
MTP 0080	J1848+0009	59846.768047	SCI-20180516-PW-01	IB	8.4	392.23	104.4	3.74	6	2	L

[a]The proposal ID of the discovery project for each source.
[b]The observing mode of the discovery observation for each source with 'CB' and 'IB' denoting coherent and incoherent beam, respectively.
[c]The total observing time in the IB and CB modes.
[d]The total number of pulses detected from each source.
[e]The number of epochs when the source was detected.
[f]The observing band at which each source has been detected.

precision is limited by the number of pulses detected and their spacing in time, and the localization accuracy of the source, we are able to obtain timing solutions for only one source.

2.4 Effelsberg follow-up

A few well-localized sources were followed up with the 100-m Effelsberg radio telescope (R. Wielebinski, N. Junkes & B. H. Grahl 2011). The observations were carried out with the Ultra Broad-Band (UBB) receiver on 2024 January 17 and 2024 February 17 with a frequency coverage of 1.3–6 GHz. The entire band was split into five subbands: 1.3–1.9 GHz, 1.9–2.6 GHz, 3.0–4.1 GHz, 4.1–5.2 GHz, and 5.2–6.0 GHz. The observations were conducted in the search mode with 8-bit full Stokes and 64 μs time resolution and 1 MHz frequency resolution. Each source was observed continuously for 2 h, and a 2 min scan of a noise diode was performed prior to each observation.

The data obtained from these observations were then searched for single pulses in the DM range of ±10 per cent of the discovery DM using TRANSIENTX[12] (Y. Men & E. Barr 2024). FILTOOL was used for RFI cleaning. We chose a DM step size of 0.1 pc cm^{-3} and a maximum boxcar width of 100 ms. Single-pulse events detected with an S/N above 8 were manually inspected for real signals. We also searched these observations with the fast folding algorithm (FFA; D. H. Staelin 1969; V. Morello et al. 2020b; S. Singh et al. 2022) as the MeerTRAP sources may emit weak regular periodic signals. We cleaned and dedispersed the data to the best DM using TRANSIENTX. Then we used the RSEEK utility of the RIPTIDE[13] package (V. Morello et al. 2020b) to search for periodic signals in the dedispersed time series. The period search range was set to ±10 per cent of the nominal period reported in Table 2, and the duty-cycle range was 0.2–20 per cent. All candidates with S/N > 8 were folded and manually inspected. Detecting regular faint periodic signals from the MeerTRAP sources would allow us to refine the period estimated by the brute-force method RRATSOLVE and study their folded pulse properties.

3 RESULTS

We present 30 new Galactic sources discovered by MeerTRAP via a single-pulse search. The discovery information of these sources is listed in Table 1, and the discovery pulses are shown in Fig. 1. We

[12]https://github.com/ypmen/TransientX

[13]https://github.com/v-morello/riptide

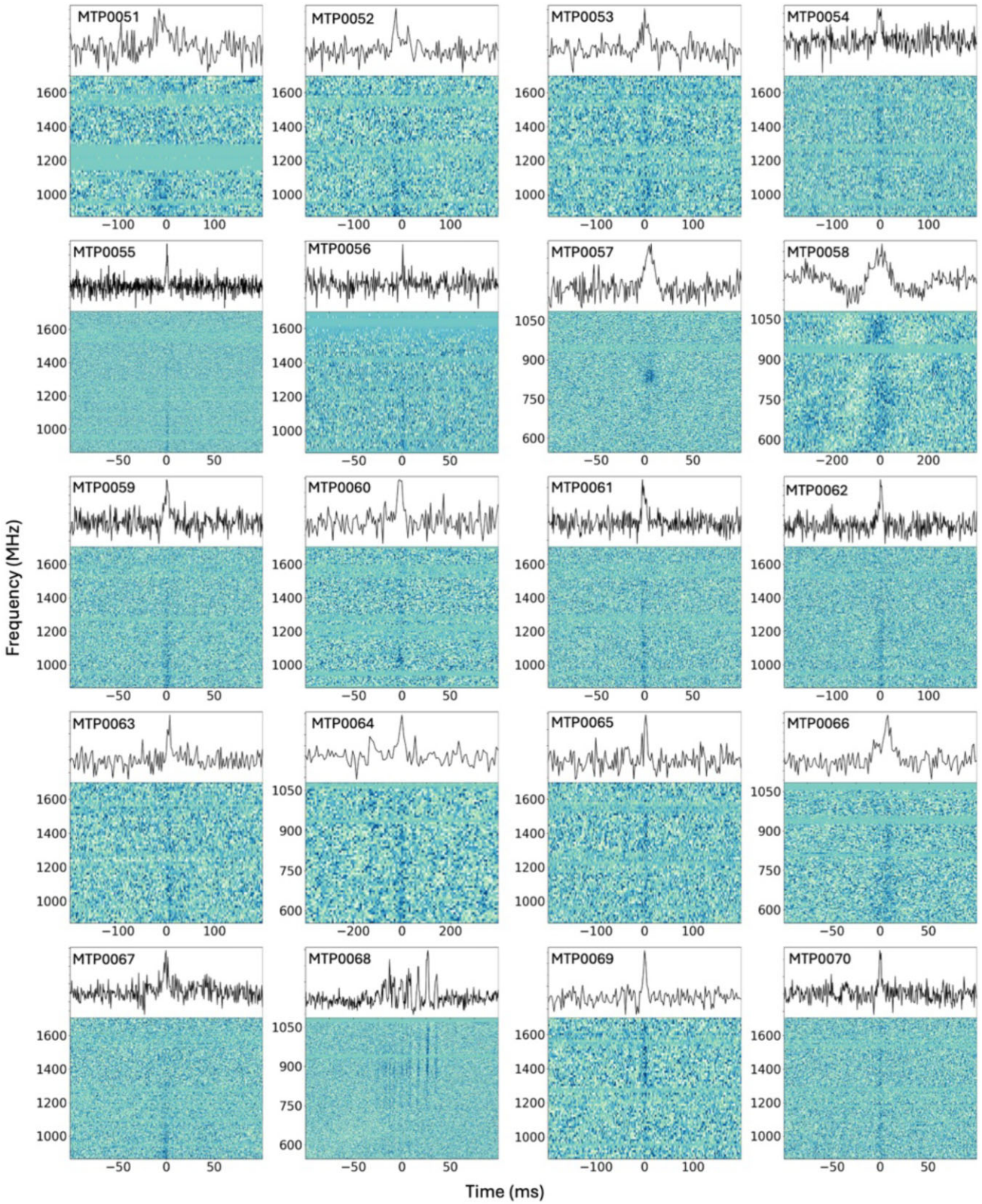

Figure 1. The discovery pulses of the 30 Galactic MeerTRAP sources. Each panel shows the dynamic spectrum (bottom) and frequency-averaged pulse profile (top) from the filterbank data dedispersed to the best DM given in Table 2. The data of faint pulses have been downsampled in frequency and time by a factor of up to 32 and 16. The source name (see Table 1) is given to each pulse in the top-left corner. Blank horizontal lines are either missing channels or flagged due to RFI. The plot of MTP 0058 is affected by RFI and zero-DM flagging.

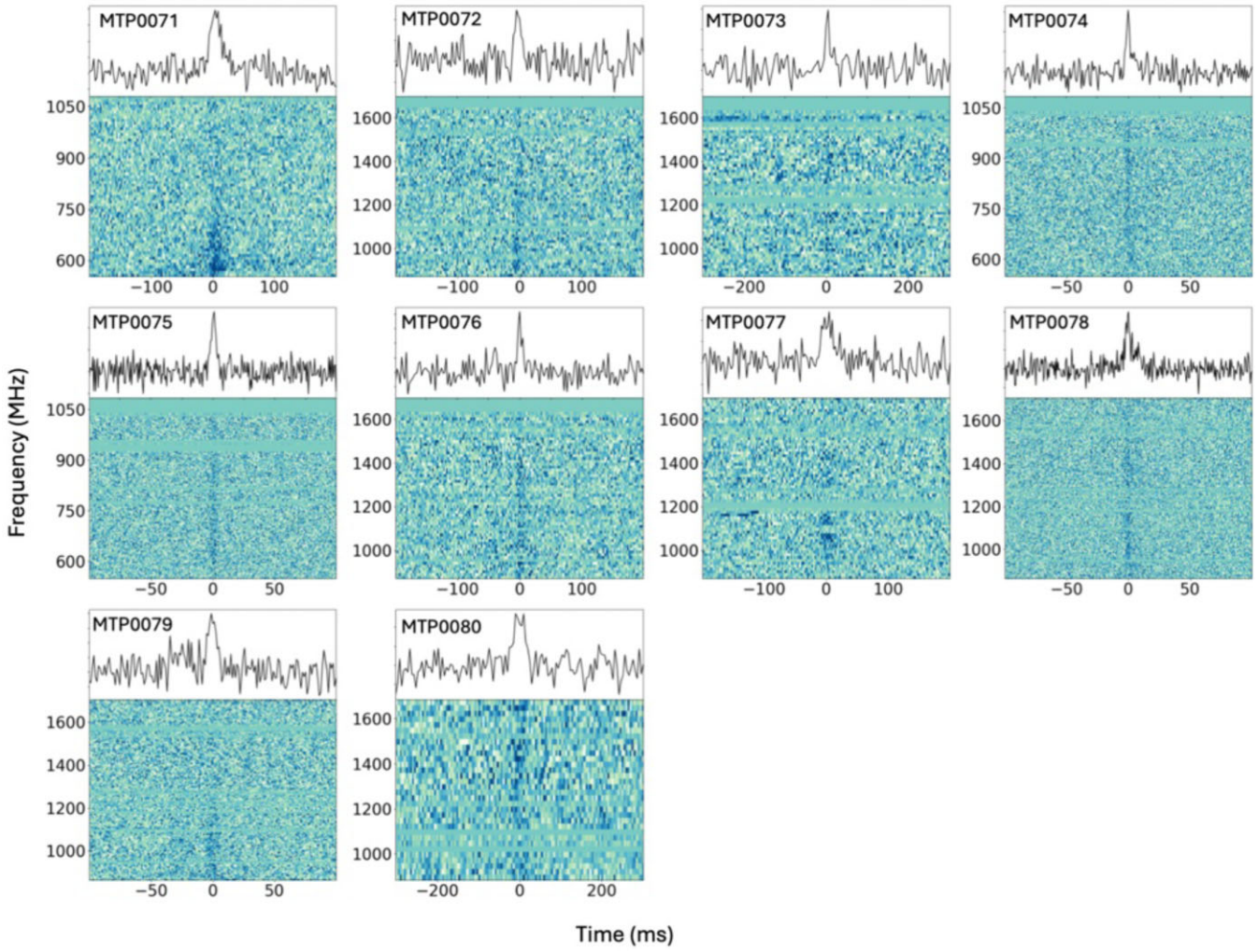

Figure 1. (*Continued.*)

note that eight of these sources were new at the time of first detection, but were independently discovered by other surveys: MTP 0067 was detected by the Max-Planck-Institut fur Radioastronomie (MPIfR)–MeerKAT Galactic Plane Survey (P. V. Padmanabh et al. 2023; see also B. W. Stappers et al. 2018); MTP 0075 was detected by the TRAPUM UHF survey for pulsars in *Fermi*-Large Area Telescope gamma-ray sources (Thongmeearkom et al., in preparation; see also C. J. Clark et al. 2023). MTP 0070 and MTP 0078 were detected by the FAST Galactic Plane Pulsar Snapshot survey (J. L. Han et al. 2025); MTP 0074 was detected by CHIME/FRB;[14] MTP 0054 was detected in the archival data of the Parkes multibeam pulsar survey (R. Sengar et al. 2023); MTP 0068 was detected by an UTMOST (V. Gupta 2022) pulsar and FRB survey (see Section 3.5); and MTP 0055 was detected by the Southern-sky MWA Rapid Two-meter (N. D. R. Bhat et al. 2023a, b) pulsar survey.[15] We highlight the eight sources in Table 1. Although these sources have been reported, we measured the properties such as the location, period, and fluence for them based on the MeerKAT data (see Table 2).

[14]The source is listed in the catalogue: http://catalog.chime-frb.ca/galactic.
[15]The source is listed in the catalogue: https://mwatelescope.atlassian.net/wiki/spaces/MP/pages/24970773/SMART+survey + candidates.

3.1 Source positions

Nine of the new Galactic sources have triggered the transient buffer and thus can be imaged using the channelized voltage data. We created and compared the on-pulse and off-pulse images of these sources and identified them in the on-pulse images, as shown in Fig. A1. After applying the astrometric correction as described in Section 2.1.3, we localized the nine sources to ∼arcsec precision, as given in Table 2. Note that the localization of MTP 0069 is significantly poorer than the other sources as the voltage data were recorded when MeerKAT was observing in the subarray mode with a maximum baseline of ∼1 km. Another four sources with more than three coherent beam (CB) detections, i.e. MTP 0057, MTP 0060, MTP 0068 and MTP 0078, were localized using SEEKAT. Their best-fitting positions along with 1σ statistical uncertainties are listed in Table 2.

MTP 0065 was triggered on a faint pulse with an S/N of 8.8, and cannot be localized in the image. Therefore, we adopted the detection beam of the brightest pulse as the position of this source and the beam size as the uncertainty, as given in Table 2.

For the other sources without voltage data or multiple CB detections, we adopted the detection beam of the brightest pulse as their position. Assuming again that the pulse detected by a single tied-array beam of MeerKAT originates within that beam, we can estimate the

Table 2. Localization, DM, distance, fluence, and period measured for each transient source. Again, the sources independently discovered by other surveys are marked with the asterisk (∗). We provide positional uncertainties for the sources localized with imaging or beam overlapping. For the other sources, their positional errors can be estimated by the beam size of the respective observing mode, i.e. ∼1 arcmin for the coherent beam and ∼1° for the incoherent beam. We do not include the distances of MTP 0051, MTP 0062, MTP 0066, and MTP 0071 because they have been detected only in incoherent beams and have large positional errors (see Section 3.1). We provide a range of fluences measured for individual pulses for the sources with imaging localization and a lower limit for the other sources, as we do not know the source location in the beam. We provide period estimates for the sources with multiple pulse detections. For the sources with only two pulse detections, we set the separation between the two pulses as the upper limit on their period.

MTP name	RA (h:m:s)	Dec. (°:′:″)	Method[a]	DM (pc cm^{-3})	$D_{<\text{NE2001/YMW16}>}$ (kpc)	Fluence (Jy ms)	P (s)	P epoch (MJD)
MTP 0051	10:46:46	−59:19:26	IB	101.1(7)		≥0.30–0.59		
MTP 0052	16:37:09	−53:26:11	CB	296(2)	6.4/13.7	≥0.26–0.41		
MTP 0053	8:44:31	−47:44:50	CB	302(1)	0.6/7.0	≥0.36		
MTP 0054*	16:55:43	−40:49:09	CB	92(1)	1.8/2.5	≥0.28		
MTP 0055*	09:17:52.9(1)	−44:20:53(1)	Imaging	45.8(1)	0.5/0.1	0.28–1.74	2.58071(3)	59835.500322
MTP 0056	15:45:43	−47:43:50	CB	86(2)	3.0/2.8	≥0.09		
MTP 0057	23:17:28(2)	−47:46:53(25)	Imaging	15.9(3)	0.7/1.8	≥0.32–0.77	1.7331602(8)	59653.481429
MTP 0058	22:18:44	−12:29:13	CB	26.8(6)	1.3/>25	≥1.36–2.28	0.1627363(1)	59673.192548
MTP 0059	9:03:34	−50:16:50	CB	150.9(3)	1.9/0.6	≥0.25		
MTP 0060	19:53:07(2)	−61:12:01(7)	Imaging	43.0(1)	1.6/4.2	≥0.11–0.46	0.46071448(3)	60607.913720
MTP 0061	16:47:30	−41:17:18	CB	35.7(3)	1.0/0.9	≥0.24–0.27		
MTP 0062	18:30:48	−10:59:28	IB	45.6(5)		≥0.24		
MTP 0063	18:17:12.6(1)	−19:32:48(2)	Imaging	214.5(2)	4.0/3.9	0.15–1.29	1.22912(2)	59769.876545
MTP 0064	16:54:02	−0:23:10	CB	65.4(6)	3.8/>25	≥0.70		
MTP 0065	17:48:14.12	−36:15:50.7	CB	266.6(5)	5.7/14.7	0.31–0.77	7.62348(5)	59747.903975
MTP 0066	6:57:26	−46:58:49	IB	148.4(4)		≥0.48–0.62		
MTP 0067*	09:33:53.2(1)	−46:04:57(1)	Imaging	120.8(1)	1.4/0.4	0.15–1.08	3.66981(6)	59782.391977
MTP 0068*	12:43:23(2)	−04:35:36(26)	Imaging	12.0(1)	0.6/1.0	≥0.40–0.79	4.86772(2)	59823.512112
MTP 0069	15:48:52.8(7)	−52:29:07(6)	Imaging	366.0(5)	7.4/6.2	0.16–0.41	≤4.85	60646.374716
MTP 0070*	19:09:49	+3:10:34	CB	110.7(4)	3.7/4.2	≥0.18		
MTP 0071	9:17:52	−44:13:20	IB	98.1(2)		≥1.04		
MTP 0072	18:31:05.1(1)	−11:41:18(1)	Imaging	46.1(2)	1.4/1.1	0.37–0.70		
MTP 0073	10:50:17	−62:22:10	CB	304(1)	6.0/2.5	≥0.23		
MTP 0074*	19:56:28.0(1)	+35:44:24(2)	Imaging	153.5(1)	6.4/7.0	0.34–1.60	0.875567(1)	59886.691847
MTP 0075*	13:03:32	−47:13:12	CB	82.6(1)	2.6/3.6	≥0.30–0.44		
MTP 0076	16:53:01	−37:45:21	CB	283(1)	5.7/15.6	≥0.23–0.33		
MTP 0077	18:40:33	−8:09:03	CB	300.0(4)	5.2/5.0	≥0.38–1.26	0.1211853(2)	60218.696604
MTP 0078*	19:14:46(2)	+2:18:13(30)	Imaging	161(1)	5.0/7.4	≥0.19–2.01	≤2.02	60292.481327
MTP 0079	18:16:39.6(1)	−24:19:01(1)	Imaging	269.4(7)	6.1/12.8	0.29–1.14	4.612833(8)	59721.920209
MTP 0080	18:48:58.3(1)	+00:09:19(1)	Imaging	393.4(4)	6.8/5.5	0.69–2.86	4.70784(8)	59972.199326

[a]We localized the sources using different methods. For those localized only in the CB or IB, their positional errors are ∼1 arcmin and ∼1°, respectively (see Section 3.1).

positional error by the beam size, i.e. ∼1 arcmin in the L band (M. C. Bezuidenhout et al. 2023). Note that for sources detected only in incoherent beams, i.e. MTP 0051, MTP 0062, MTP 0066, and MTP0071, their positional errors are much larger (∼deg). All source positions are listed in Table 2.

We derived the distances of the MeerTRAP sources based on the `NE2001` (J. M. Cordes & T. J. W. Lazio 2002) and `YMW16` (J. M. Yao, R. N. Manchester & N. Wang 2017) Galactic electron density models, as given in Table 2. Note that we do not provide distances for the sources detected only in incoherent beams due to their large positional errors. As can be seen, there are large discrepancies in the distance estimates from these two models for some of the sources. Specifically, the sources located close to the Galactic anticentre and at low Galactic latitudes are predicted to be more distant by `NE2001` than by `YMW16`. This is consistent with the findings from the comparison of the two models (D. C. Price, C. Flynn & A. Deller 2021). Interestingly, MTP 0058 and MTP 0064 have DMs slightly higher than the Galactic contribution predicted by `YMW16`. However, given that `YMW16` does not model the DM contribution from the Galactic halo, which amounts to ∼40–60 pc cm^{-3} along the line of sight (S. Yamasaki & T. Totani 2020), we still consider these two sources to be of Galactic origin.

3.2 Timing solutions

We measured the periods of the MeerTRAP sources with multiple pulses detected closely in time, as listed in Table 2. As MTP 0069 and MTP 0078 had only two pulses detected in quick succession, we set upper limits on their periods based on the separation between the two pulses. For the sources with pulse detections over a long time span, we used TEMPO2 to compare the TOAs against the initial period and imaging localization, and obtained a phase-connected timing solution for MTP 0063. Due to the limited data available for MTP 0063, we did not fit any timing parameters other than the period and period derivative. The best-fitting timing solution is given in Table 3, and the timing residuals are shown in Fig. 2. The period derivative is poorly constrained due to the limited time span of the TOAs. The distribution of the timing residuals, as shown in the right panel of Fig. 2, suggests two components separated by ∼50 ms in the average profile of MTP 0063. As the radio emission switched between the two components, our methodology of fitting a single Gaussian to the pulse generated the TOA of either the first or the second component. This causes the gap between two sets of TOAs, as can be seen in Fig. 2. This is similar to that observed in some other RRATs discovered by MeerTRAP, e.g. PSRs J1911−2020 and J1930−1856 (J. D. Turner

Table 3. Timing solution for MTP 0063.

Fit and data set	
PSR name	J1817−1932
MeerTRAP name	MTP 0063
MJD range	59739–59776
Number of TOAs	128
rms timing residual (ms)	16.8
Weighted fit	Y
Reduced χ^2	780
Measured quantities	
Right ascension, α (^{h}:^{m}:^{s})	18:17:12.6(1)
Declination, δ ($^{\circ}$:$'$:$''$)	−19:32:48(2)
Spin period, P (s)	1.229084876(7)
First derivative of P, $\dot{P}$ ($\times 10^{-15}$ s s^{-1})	1(5)
Epoch of period determination (MJD)	59769.9
Epoch of position determination (MJD)	59769.9
Epoch of DM determination (MJD)	59769.9
Dispersion measure, DM (cm^{-3} pc)	214.5(2)
Assumptions	
Clock correction procedure	TT(TAI)
Solar system ephemeris model	DE405
Binary model	None
Model version number	5.00

et al. 2025), and the magnetar-like PSR J1819−1458 (A. G. Lyne et al. 2009; B. Bhattacharyya et al. 2018).

3.3 Fluences

We estimated the fluence of individual pulses based on the modified single-pulse radiometer equation (e.g. F. Jankowski et al. 2023). This included the calculation of the system equivalent flux density of the MeerKAT array and the array's beam response at the source position. More details can be found in J. Tian et al. (2024). The range of fluences measured for individual pulses for each source is given in Table 2. Note that for the sources without imaging localization, as we do not know their location in the beam, we provide only a lower limit on their fluence. In Fig. 3, we plot the fluence distribution for the sources with >20 pulses observed by MeerKAT and with an imaging localization. MTP 0055 has 17 pulses detected at UHF and 9 pulses at L band, while the other three sources are all at L band. The fluences of the four sources seem to follow a lognormal-like distribution with a peak at ∼0.3–0.7 Jy ms, as shown by the best-fitting lognormal distribution in Fig. 3. Previous studies of RRAT pulses also found their fluences to be lognormally distributed (S. Burke-Spolaor et al. 2011; B. W. Meyers et al. 2018, 2019). We note that the fluence distributions presented here could be biased due to the MeerTRAP survey performance and completeness limit. Given the limited small sample of pulses from the MeerTRAP sources, we cannot obtain the exact fluence distribution here.

3.4 Polarization of single pulses

For the nine sources that triggered voltage buffer dumps, we have polarization information. However, many of these sources are very faint, and it is hard to get reliable polarization information and rotation measure (RM) measurements. Here, we present polarized flux only for those sources with S/N > 15 in the detected pulse, i.e. MTP 0063, MTP 0067, MTP 0072, and MTP 0074. To measure their polarization, we calibrated the voltage data by applying the primary beam Jones matrix derived from MeerKAT holography experiments (M. S. Villiers 2023). A detailed description of the polarization calibration is given in K. M. Rajwade et al. (2024).[16] Note that this method may be inaccurate as there is no measurement of the Jones matrix at the time of the trigger. We therefore added 5 per cent uncertainty to the measurement of polarization fractions to account for any residual leakage.

After the calibration, we used the pulsar software PSRSALSA[17] (P. Weltevrede 2016) to measure the RM and polarization fraction. We followed the same procedure as described in J. Tian et al. (2024). The polarimetric pulse profiles of the four MeerTRAP sources are shown in Fig. 4, and the measured RM and linear and circular polarization fractions are given in Table 4. The pulse of MTP 0063 is highly polarized with a linear and circular polarization fraction of $L/I = 0.79 \pm 0.13$ and $|V|/I = 0.26 \pm 0.09$. The other three pulses are less polarized. We see variations of polarization position angles (PPAs) across these pulse profiles, e.g. sweeping down in MTP 0072 and MTP 0074 and sweeping up in MTP 0063. Such PPA variations are reminiscent of pulsar emission produced in the pulsar magnetosphere (e.g. J. L. Han et al. 2021).

3.5 UTMOST detection of MTP 0068

A source with properties similar to MTP 0068 was detected in FRB 'Survey V', carried out at UTMOST, via its single-pulse detection pipeline (V. Gupta 2022). The source was detected in a 15-min drift scan observation. The UTMOST survey strategy was to tile its $4^{\circ} \times 2^{\circ}$ field of view with 352 fine stationary phased-array-beams (termed 'fan-beams'). Each fan-beam was independently searched for single pulses in real-time, as the sky drifted through them. On 2019 June 18, we detected three pulses from an uncatalogued source. Our analysis showed it was moving across the fan-beams at the sky drift rate. At a detection DM of 11.5 pc cm^{-3}, the DM of the pulses was well below the DM cut-off for which raw voltage data would be triggered and retained. Subsequently, lower time-resolution 'search-mode' data (which is retained) were analysed offline. The discovery pulse is shown in Fig. 5. The best-fitting sky position, consistent for all three pulses, was found to be RA = 12:43:23.6 ± 45″ and Dec. = −05:34:23.2 ± 2°. Due to the alignment of the UTMOST array along the east–west axis, the precision in localization is high in the RA direction (∼45 arcsec), but quite poor in the Dec. direction (∼2°). Using the fan-beam filterbanks of all beams within the field of view, we stitched together a tied-array beam filterbank that tracked the best-fitting position of the source on the sky. We then conducted a search for periodicity using the RIPTIDE implementation of the FFA (V. Morello et al. 2020b) and obtained an 11σ detection of a 4.86 s periodicity for the source. Given the DM, location and period of this previously uncatalogued source discovered by UTMOST are all consistent with MTP 0068, we consider them to be the same source.

3.6 Microstructure of MTP 0068

Most of the sources reported in this paper have simple morphology with either one or two distinct components. However, MTP 0068 (J1243−0435) shows interesting pulses with many subcomponents. It was discovered by MeerKAT on 2022 September 1 with five pulses detected within ∼30 min in the UHF. It has a small DM below the 20 pc cm^{-3} threshold, and yet was detected (that is why the

[16]The code for performing the polarization calibration can be found on GitLab: https://gitlab.com/kmrajwade/tbeamformer.
[17]https://github.com/weltevrede/psrsalsa

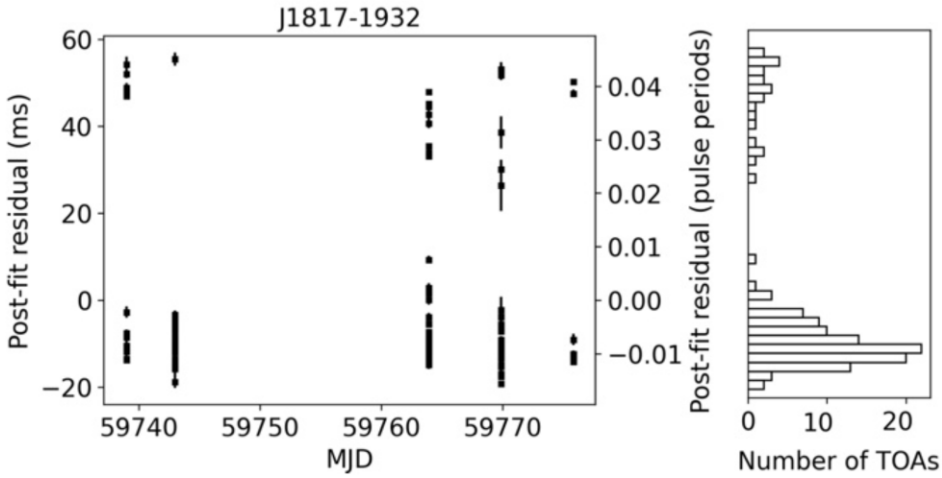

Figure 2. Best-fitting timing residuals of MTP 0063/PSR J1817−1932 (left) and distribution of residuals (right).

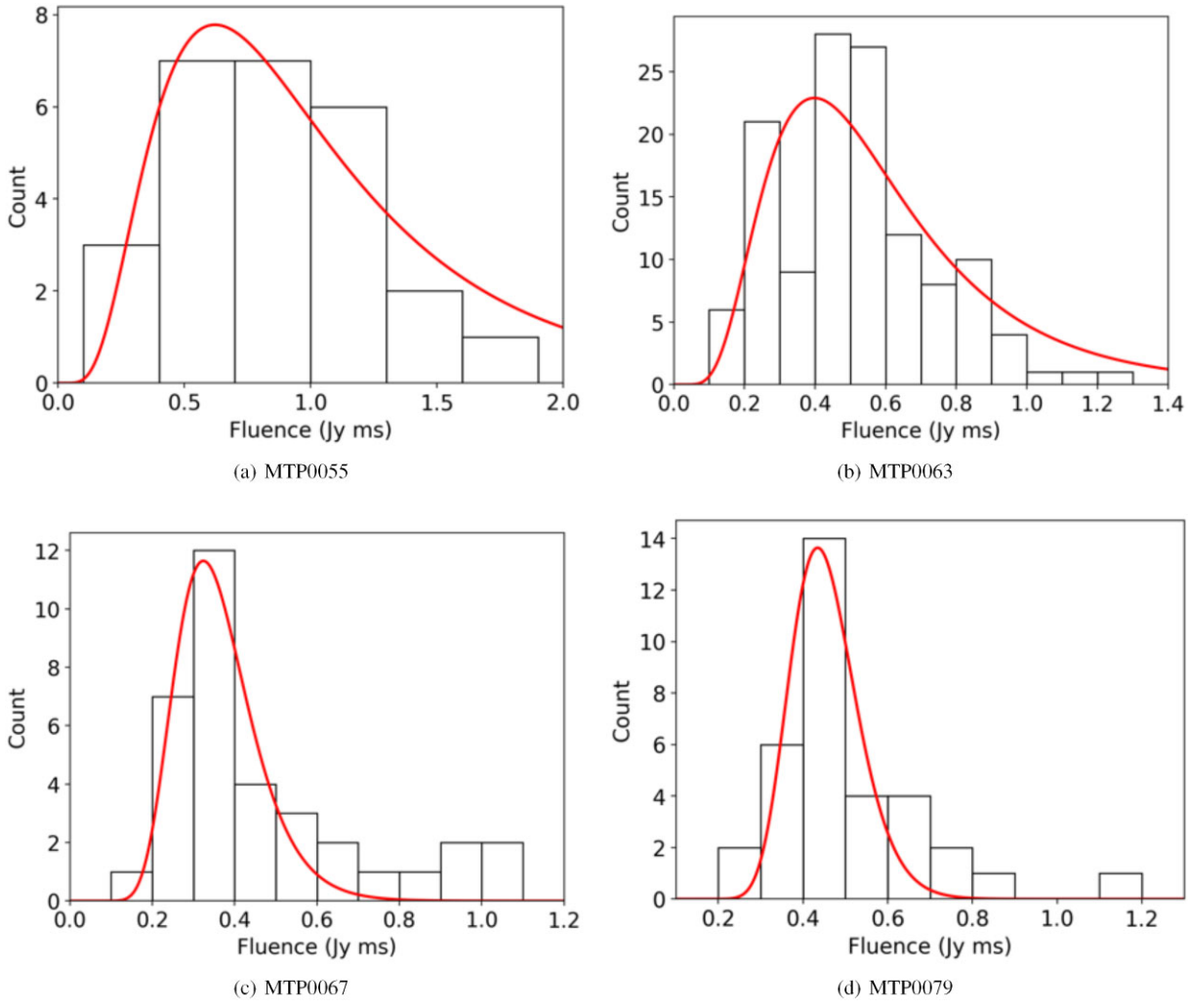

Figure 3. Fluence distributions of individual pulses for the MeerTRAP sources with imaging localization and more than 20 pulse detections. MTP 0055 is detected in both UHF (17 pulses) and L band (nine pulses), while the other three sources are detected only in the L band. The red line shows the best-fitting lognormal distribution for the observed pulse fluences of each source.

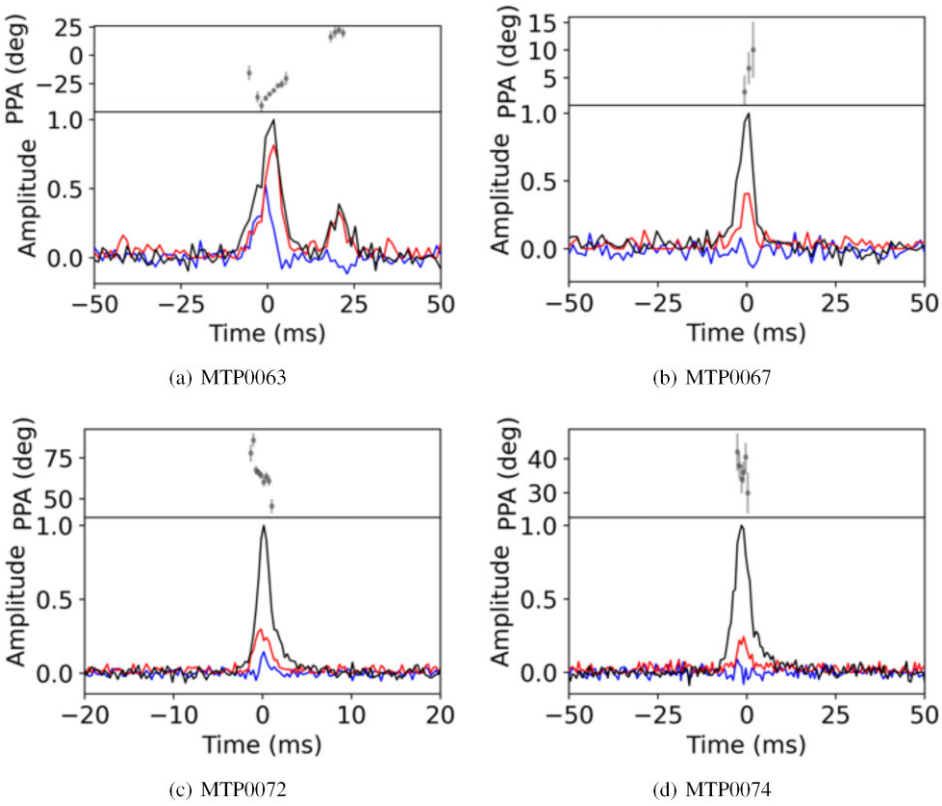

Figure 4. Polarization profiles of bright pulses created from the transient buffer data. Each panel shows the PPA (top) and the frequency-averaged pulse profile (bottom) for total intensity (I, black), linear polarization (L, red), and circular polarization (V, blue). The polarization data are Faraday corrected to the RM values given in Table 4. Vertical error bars indicate the 1σ uncertainties in the PPA.

Table 4. Polarization properties of bright pulses for the MeerTRAP sources with transient buffer data.

MTP name	RM (rad m^{-2})	L/I	$\lvert V\rvert/I$
MTP 0063	347(1)	0.79(13)	0.26(9)
MTP 0067	76(3)	0.41(12)	0.14(10)
MTP 0072	30(2)	0.43(10)	0.08(8)
MTP 0074	193(1)	0.21(7)	0.06(6)

discovery DM in Table 1 is 21.49 pc cm^{-3} compared to the true DM of 12 pc cm^{-3} given in Table 2) due to its brightness and complex substructure. As none of the pulses triggered transient buffer data, we utilized the overlap between the detection CBs to constrain the source position. An initial period of 4.867 s was found using the TOAs of the five pulses, and later confirmed using the Effelsberg follow-up observation (see Section 3.7). This source was also observed by MeerKAT on 2020 September 11 for ∼1 h and on 2022 December 17 for ∼1 h, but no pulse was detected. This might reflect the clustering of sporadic strong pulses in time.

The pulses from MTP 0068 (J1243−0435) show quasi-periodic narrow emission components, known as microstructure (T. H. Hankins 1996; D. Mitra, M. Arjunwadkar & J. M. Rankin 2015). Microstructure is commonly seen in pulsars, radio magnetars, RRATs, and sometimes even in long-period transients and FRBs (M. Caleb et al. 2022; I. Pastor-Marazuela et al. 2023; M. Kramer et al. 2024). We only analysed one bright pulse from J1243−0435 (Fig. 6, left panel) for microstructure quasi-periodicity; the others were too faint. We computed the power spectrum of the pulse and

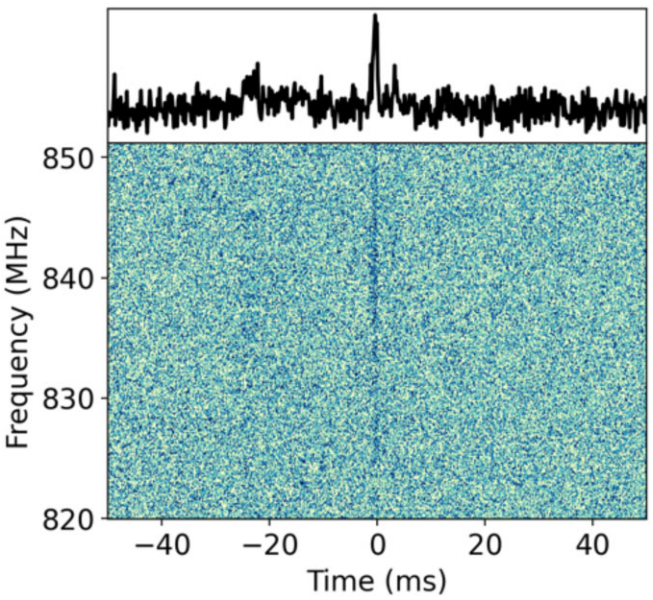

Figure 5. The discovery pulse of MTP 0068 at UTMOST. The top panel shows the frequency-averaged pulse profile, while the bottom panel shows the dynamic spectrum. The data have been dedispersed to the detection DM of 11.5 pc cm^{-3}.

identified a peak at 118.6 Hz, as shown in the right panel of Fig. 6. This peak corresponds to a period of $P_\mu = 8.4^{+1.2}_{-0.6}$ ms, where the uncertainty is determined by the full width at half-maximum of

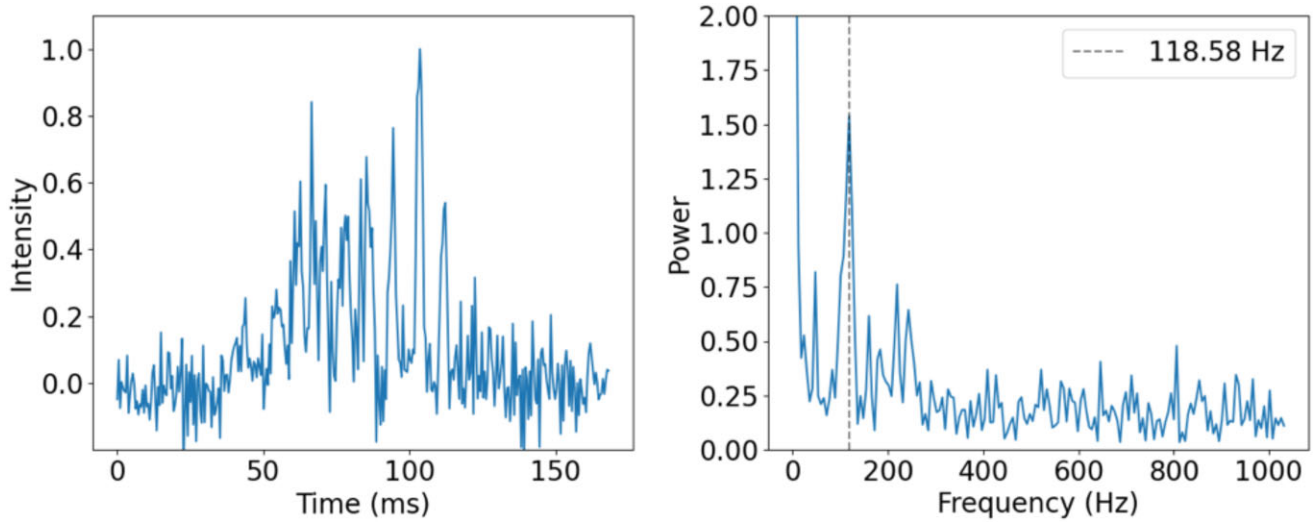

Figure 6. Microstructure in a pulse detected from J1243−0435 on 2022 September 1. The left panel shows the pulse shape, while the right panel shows the power spectrum of the pulse. We find a 3σ peak in the power spectrum at a frequency of $118.6^{+9.6}_{-14.4}$ Hz, corresponding to a microstructure periodicity of $8.4^{+1.2}_{-0.6}$ ms.

the peak. Considering the rotation period of this source $P = 4.87$ s, the microstructure periodicity obtained here is consistent with the empirical relation $P_\mu \sim 10^{-3} P$ known for radio-emitting neutron stars (M. Kramer et al. 2024).

In order to assess the significance of this periodicity, we fitted the pulse profile with a multicomponent Gaussian model. We allowed the number of components to vary between 7 and 13 and selected the model with the lowest BIC, which in this case corresponded to 10 components. We fitted the arrival time as a function of component number to a linear function, allowing gaps between components, to find the mean intercomponent wait-time. Using this mean wait-time, we simulated pulses following a Poissonian wait-time distribution with the same mean spacing as the observed pulses. To prevent simulated components from clustering too closely, we enforced a minimum separation equal to 0.2 times the mean intercomponent time, which we refer to as the exclusion parameter, or η. We then generated 10^5 simulated sets of TOAs, and found that 99.881 per cent of the simulations had larger reduced χ^2 than the tested periodicity. This corresponds to a significance of 3.24σ, which means that the fitted quasi-periodicity is not readily explained by the null hypothesis of Poisson-distributed pulses. More details about the timing technique can be found in I. Pastor-Marazuela et al. (2023).

3.7 Persistent emission and folded profiles

The new sources presented here were found in the real-time MeerTRAP single-pulse search. The pipeline detected relatively low number of pulses from most sources, despite extended observation periods when they were in the field of view (see Table 1). However, there could be more regular but weaker emissions from these sources. In order to find this regular weak signal, we searched the follow-up observations with Effelsberg (see Section 2.4) of five long-period ($P \geq 4$ s) MeerTRAP sources. Three of these sources, PSRs J1911−2020, J1525−2322, and J2218+2902, have been published in J. D. Turner et al. (2025) and the other two sources, PSRs J1243−0435 (MTP 0068) and J1816−2419 (MTP 0079), are reported here.

We found regular periodic signals in the follow-up observations of three sources, PSRs J1911−2020, J2218+2902, and J1243−0435. Fig. 7 shows the phase versus time plot along with the folded profile of these sources, and Table 5 lists the duty cycles measured for them. We can see hints of nulling features in the time–phase plot of these sources. However, due to the limited S/N, we do not measure the nulling fraction here.

4 DISCUSSION

4.1 Interesting sources

Many of the MeerTRAP sources have been detected only a few times despite the large amount of observing time in the incoherent beam (IB) mode at MeerKAT, as can be seen in Table 1. This could be due to an intrinsically low activity of these sources or their pulses being too faint to be detected by the IB mode. More sensitive follow-ups are needed to confirm whether these sources are genuinely inactive or their pulses are too faint.

A few of the Galactic sources presented here exhibit unusual properties. PSR J2218+2902 was initially reported in J. D. Turner et al. (2025). There are only a few slow pulsars discovered so far, including PSR J0250+5854 ($P = 23.5$ s; C. M. Tan et al. 2018), PSR J0901−4046 ($P = 76$ s; M. Caleb et al. 2022), and PSR J0311+1402 ($P = 41$ s s; Y. Wang et al. 2025). Searching for more of them is important as they can be used to constrain the pulsar emission mechanism and provide new insights into the neutron star evolution path. Our follow-up of PSR J2218+2902 with Effelsberg found faint periodic emission with a period of 17.49 s (see Fig. 7). Therefore, we confirm PSR J2218+2902 to be the fourth slowest in the radio pulsar population.

Three out of the five sources we have followed up with Effelsberg turn out to be also detectable as apparently normal pulsars. These three sources are all located below the Galactic plane with $|b| > 10^\circ$ and thus not covered by Galactic plane pulsar surveys (e.g. R. N. Manchester et al. 2001; J. M. Cordes et al. 2006; J. W. T. Hessels et al. 2008; E. F. Keane et al. 2018). PSRs J1911−2020 and J1243−0435 are within the region of the HTRU-South survey,

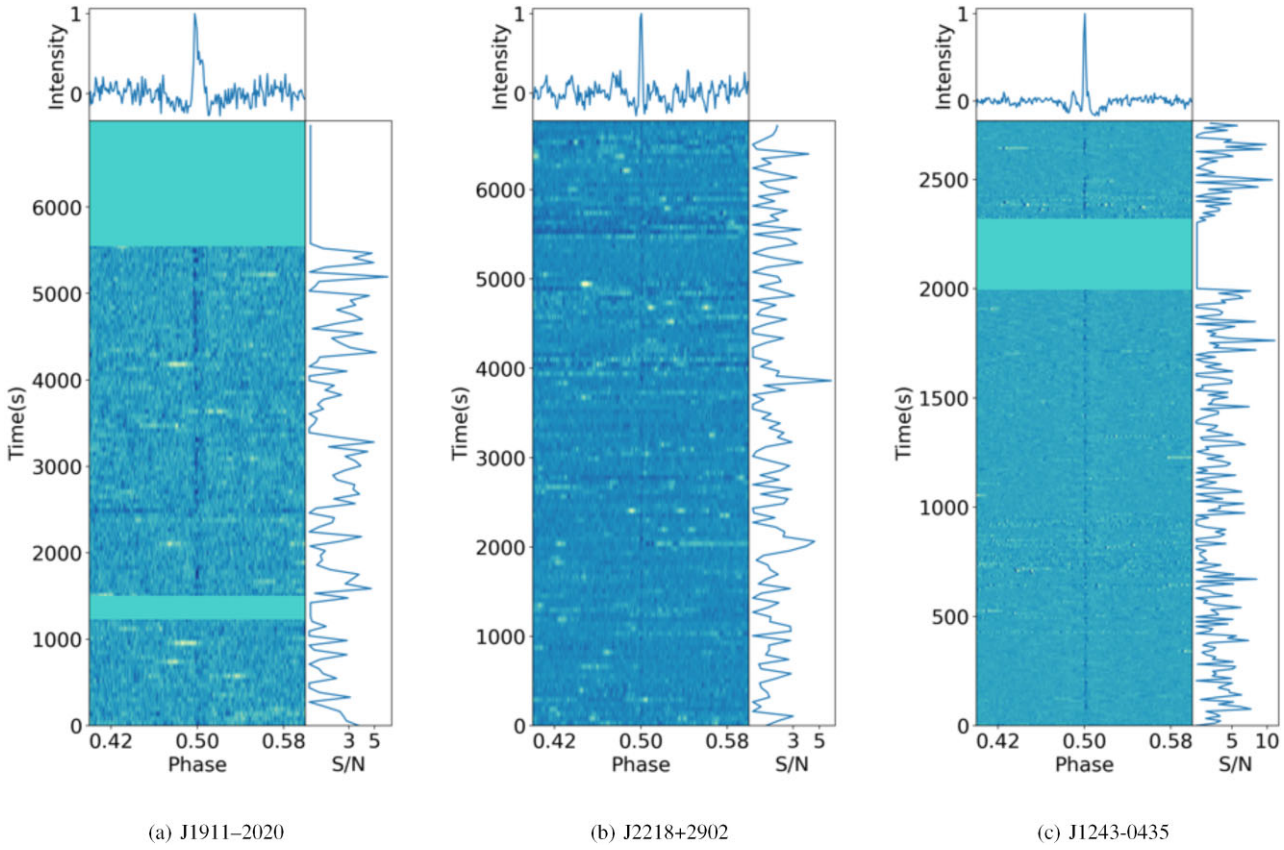

Figure 7. Three MeerTRAP sources detected in the Effelsberg follow-up observations. For each source, the main left panel shows the pulse-stack in the phase–time space, and the top panel shows the averaged pulse profile. The right panel shows the evolution of S/N with time, with the noise calculated from the off-pulse region. Blank horizontal lines in the time–phase plot represent intervals masked due to RFI. The pulsed emission of the three sources is intermittent and shows hints of nulling features.

Table 5. Duty cycle and S/N of the pulsed emission measured for the three MeerTRAP sources shown in Fig. 7.

PSR name	Duty cycle (per cent)	S/N
J1911−2020	(0.84 ± 0.10)	20.9
J2218+2902	(0.29 ± 0.10)	27.4
J1243−0435	(0.21 ± 0.02)	81.4

which targets the entire sky south of declination of $+10^{\circ}$ (M. J. Keith et al. 2010). However, these two sources were not discovered in this survey, probably because of the red noise in the data, which reduced the sensitivity to pulsars with a spin period above 500 ms or the flux density of the two sources being below the survey sensitivity. It is possible that some other Galactic sources discovered by MeerTRAP are pulsars with very sparse bright pulses as well. Continuous follow-up of more MeerTRAP sources would reveal more pulsars in the apparent RRAT population and enable studies of their pulse energy distributions and further elucidate the nature of this population of radio-emitting neutron stars and how they fit in with the more steady emitting pulsars.

We note the extended source to the north of MTP 0079 is the supernova remnant (SNR) G7.7−3.7 (see e.g. W. D. Cotton et al. 2024). We briefly investigated whether MTP 0079 and G7.7−3.7 could have been produced by the same supernova event. This scenario would mean MTP 0079 is much younger than other neutron stars discovered by MeerTRAP. The lifetime of radio-detected SNRs is typically $\lesssim$80 kyr (D. A. Frail, W. M. Goss & J. B. Z. Whiteoak 1994; J. Vink 2020), and G7.7−3.7 has been suggested to be a possible remnant of the supernova of AD 386 (P. Zhou et al. 2018). The offset of MTP 0079 from the geometric centre of G7.7−3.7 is $\approx$18.2 arcmin. Assuming the `NE2001` distance of 6.1 kpc for MTP 0079, its birth velocity would be unprecedentedly large ($\sim 2 \times 10^4$ km s^{-1}) if it was associated with the supernova of AD 386. However, the derived velocity may be wrong given that G7.7−3.7 has not been extensively studied and its age is very uncertain. However, this region near the Galactic plane is a highly populated area of the sky. Therefore, measurements of the proper motion of MTP 0079 would be needed to firmly establish an association.

4.2 Future prospects

The discoveries reported here and in M. C. Bezuidenhout et al. (2022) and J. D. Turner et al. (2025) demonstrate the capability of the single-pulse search program with the sensitive telescope MeerKAT. Such a campaign can not only increase the population of FRBs but also significantly contribute to the population of Galactic transients. While fast Fourier transform based periodicity searches have discovered the majority of known pulsars, they are known to be less sensitive towards pulsars with long periods and/or small duty cycles (E. Heerden, A. Karastergiou & S. J. Roberts 2017; V. Morello et al. 2020b). An alternative periodicity search method, called the FFA search (D. H. Staelin 1969), provides better sensitivity for pulsars with long periods and small duty cycles (V. Morello et al.

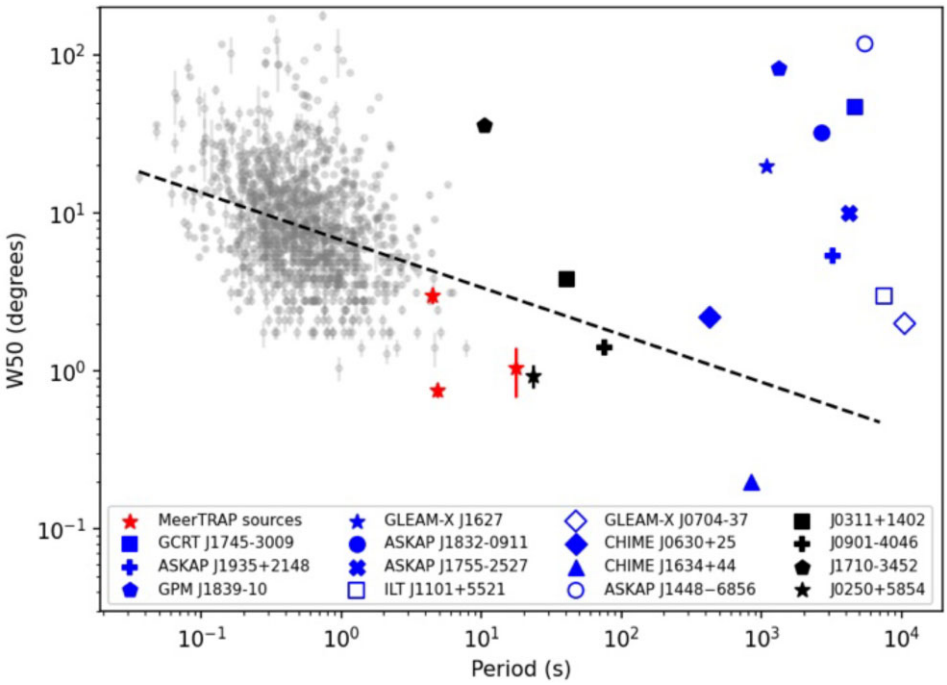

Figure 8. Duty cycle versus pulsar period. The grey dots represent pulsars from the Thousand-Pulsar-Array programme on MeerKAT (B. Posselt et al. 2021), the black points represent the three long-period pulsars (C. M. Tan et al. 2018; M. Caleb et al. 2022; M. P. Surnis et al. 2023; Y. Wang et al. 2025), the blue points represent the ULP transients (S. D. Hyman et al. 2005; N. Hurley-Walker et al. 2022, 2023, 2024; M. Caleb et al. 2024; A. Anumarlapudi et al. 2025; F. A. Dong et al. 2025a, b; S. J. McSweeney et al. 2025; I. Ruiter et al. 2025; Z. Wang et al. 2025a), and the red points represent the three MeerTRAP sources with persistent emission observed by Effelsberg (see Section 3.7). We indicate the ULPs with optical counterparts in empty markers. The dashed line shows the empirical relation $W \propto P^{-0.3}$ between the observed profile width and pulsar spin period (S. Johnston & A. Karastergiou 2019).

2020b; S. Singh et al. 2022). The FFA search is also believed to be more sensitive towards highly nulling pulsars (S. Singh et al. 2023; G. Grover, R. Bhat & S. McSweeney 2024). However, these periodicity search methods may still miss weak pulsars with occasional bright pulses, as demonstrated by D. J. Zhou et al. (2023). These pulsars are more likely to be detected by single-pulse searches like those used by MeerTRAP and other projects searching for FRBs. In addition, we have discovered some sources with long periods and small duty cycles. Fig. 8 shows the duty cycle of these sources, in comparison with radio pulsars (B. Posselt et al. 2021), long-period pulsars (C. M. Tan et al. 2018; M. P. Surnis et al. 2023; Y. Wang et al. 2025), and ULP transients (S. D. Hyman et al. 2005; M. Caleb et al. 2022, 2024; N. Hurley-Walker et al. 2022, 2023, 2024; A. Anumarlapudi et al. 2025; F. A. Dong et al. 2025a, b; S. J. McSweeney et al. 2025; I. Ruiter et al. 2025; Z. Wang et al. 2025a). As can be seen, the duty cycles of the MeerTRAP sources are very low, which might imply a narrow pulsar beam, however this depends on the viewing geometry. While the long-period pulsars follow the general trend for the duty cycle with period (K. Maciesiak, J. Gil & G. Melikidze 2012; A. Skrzypczak et al. 2018; B. Posselt et al. 2021), the ULP transients look like they are outliers and some of them may not be neutron stars, but white dwarf binaries, e.g. GLEAM-X J0704−37 and ILT J1101+5521 (N. Hurley-Walker et al. 2024; I. Ruiter et al. 2025). With MeerTRAP, we expect to discover more long-period pulsars that are located in the gap between pulsars and long-period transients, which would further reveal their relationships.

The results from the follow-up observations presented here motivate us to follow up more Galactic transients discovered by MeerTRAP with other telescopes. These follow-up observations will help us obtain a coherent timing solution, allowing us to determine their spin-down rate, magnetic field strength, and characteristic age, potentially placing these discoveries in the underpopulated regions of the P–$\dot{P}$ diagram (e.g. the magnetar regime or the pulsar death valley). As can be seen in this work, the long continuous observations can sometimes reveal weak regular emission from the apparently transient sources. Follow-up with sensitive telescopes may also allow us to study their emission properties in greater detail.

5 CONCLUSIONS

In this paper, we have presented 30 new Galactic sources the MeerTRAP project discovered in real-time via a single-pulse search. This work, along with that published by M. C. Bezuidenhout et al. (2022) and J. D. Turner et al. (2025), has demonstrated the efficiency of MeerTRAP in finding Galactic transient sources. Most of these sources are likely to be RRATs given their low pulse rates. We localized nine of the MeerTRAP sources to arcsecond precision using the voltage buffer data, and obtained a phase-coherent timing solution for MTP 0063/PSR J1817−1932. We estimated the fluence distribution of single pulses for four of the MeerTRAP sources. The fluences range between ∼0.1 and 2 Jy ms with a peak at ∼0.3–0.7 Jy ms, and might follow a lognormal distribution. We also measured polarization properties of single pulses for four of the MeerTRAP sources, and found them to be linearly polarized with a polarization fraction up to 79 per cent. We also investigated the microstructure observed in PSR J1243−0435. A period of $8.4^{+1.2}_{-0.6}$ ms was identified at 3σ significance in the brightest pulse from PSR J1243−0435. This microstructure periodicity and the spin period of the source follow the universal relation previously seen in

radio-emitting neutron stars (M. Kramer et al. 2024). In addition, we found regular faint emission from three sources using the Effelsberg follow-up observations. This confirms their long rotation period, including PSR J2218+2902 with a period of 17.5 s. Considering the ongoing transient search with MeerTRAP, we expect to discover more RRATs and pulsars, especially those with long rotation periods.

ACKNOWLEDGEMENTS

The MeerKAT telescope is operated by the South African Radio Astronomy Observatory (SARAO), which is a facility of the National Research Foundation, itself an agency of the Department of Science and Innovation. All the authors thank the MeerKAT LSP teams, including MALS, MeerTime, MHONGOOSE, and ThunderKAT, for allowing commensal observing and the staff at SARAO for scheduling MeerKAT observations. MeerTRAP observations use the FBFUSE and TUSE computing clusters for data acquisition and storage. These instruments were designed, funded, and installed by the Max-Planck-Institut für Radioastronomie (MPIfR) and the Max-Planck-Gesellschaft. This publication includes data from observations with the 100-m telescope of the MPIfR at Effelsberg. The Effelsberg UBB receiver and EDD system are developed and maintained by the electronics division at the MPIfR. The authors are thankful to Dr Alex Kraus for scheduling the observations. MeerTRAP acknowledges funding from the European Research Council (ERC) under the European Union's Horizon 2020 Framework Programme (grant agreement no. 694745). JT and BWS acknowledge funding from an STFC consolidated grant. JDT acknowledges funding from the UK Research and Innovation and Science and Technology Facilities Council (STFC) Doctoral Training Partnership, project code 2659479. MC acknowledges support of an Australian Research Council Discovery Early Career Research Award (project number DE220100819) funded by the Australian Government. IP-M further acknowledges funding from an NWO Rubicon Fellowship, project number 019.221EN.019. For the purpose of open access, the author has applied a Creative Commons Attribution (CC BY) licence to any Author Accepted Manuscript version arising. This research used version 2.2.0 of the ATNF Pulsar Catalogue. This research has made use of the SIMBAD data base, operated at CDS, Strasbourg, France (M. Wenger et al. 2000). This research has made use of NASA's Astrophysics Data System Bibliographic Services.

DATA AVAILABILITY

The data underlying this article will be shared on reasonable request to the corresponding authors.

REFERENCES

Anumarlapudi A. et al., 2025, MNRAS, 542, 1208
Archibald R. F. et al., 2017, ApJ, 849, L20
Barr E. D. et al., 2013, MNRAS, 435, 2234
Beskin V. S., Chernov S. V., Gwinn C. R., Tchekhovskoy A. A., 2015, Space Sci. Rev., 191, 207
Bezuidenhout M. C. et al., 2022, MNRAS, 512, 1483
Bezuidenhout M. C. et al., 2023, RAS Tech. Instrum., 2, 114
Bhat N. D. R. et al., 2023a, Publ. Astron. Soc. Aust., 40, e020
Bhat N. D. R. et al., 2023b, Publ. Astron. Soc. Aust., 40, e021
Bhattacharyya B. et al., 2018, MNRAS, 477, 4090
Bhattacharyya B. et al., 2019, ApJ, 881, 59
Bochenek C. D., Ravi V., Belov K. V., Hallinan G., Kocz J., Kulkarni S. R., McKenna D. L., 2020, Nature, 587, 59
Burke-Spolaor S. et al., 2011, MNRAS, 416, 2465
Caleb M. et al., 2019, MNRAS, 487, 1191
Caleb M. et al., 2022, Nat. Astron., 6, 828
Caleb M. et al., 2023, MNRAS, 524, 2064
Caleb M. et al., 2024, Nat. Astron., 8, 1159
Chen W., Barr E., Karuppusamy R., Kramer M., Stappers B., 2021, J. Astron. Instrum., 10, 2150013
Chen J. L. et al., 2022, ApJ, 934, 24
CHIME Collaboration, 2022, ApJS, 261, 29
CHIME/FRB Collaboration, 2018, ApJ, 863, 48
CHIME/FRB Collaboration, 2019, ApJ, 885, L24
CHIME/FRB Collaboration, 2020, Nature, 587, 54
Clark M. A., La Plante P. C., Greenhill L. J., 2011, preprint (arXiv:1107.4264)
Clark C. J. et al., 2023, MNRAS, 519, 5590
Cordes J. M., Lazio T. J. W., 2002, preprint (arXiv:astro-ph/0207156)
Cordes J. M., McLaughlin M. A., 2003, ApJ, 596, 1142
Cordes J. M. et al., 2006, ApJ, 637, 446
Cotton W. D., Kothes R., Camilo F., Chandra P., Buchner S., Nyamai M., 2024, ApJS, 270, 21
Dang S. J. et al., 2024, MNRAS, 528, 1213
Deller A. T., Tingay S. J., Bailes M., West C., 2007, PASP, 119, 318
Deller A. T. et al., 2011, PASP, 123, 275
de Ruiter I. et al., 2025, Nat. Astron., 9, 672
de Villiers M. S., 2023, AJ, 165, 78
Dong F. A. et al., 2023, MNRAS, 524, 5132
Dong F. A. et al., 2025a, ApJ, 988, L29
Dong F. A. et al., 2025b, ApJ, 990, L49
Driessen L. N. et al., 2022, MNRAS, 512, 5037
Driessen L. N. et al., 2024, MNRAS, 527, 3659
Eatough R. P., Keane E. F., Lyne A. G., 2009, MNRAS, 395, 410
Frail D. A., Goss W. M., Whiteoak J. B. Z., 1994, ApJ, 437, 781
Good D. C. et al., 2021, ApJ, 922, 43
Grover G., Bhat R., McSweeney S., 2024, Publ. Astron. Soc. Aust., 41, e046
Gupta V., 2022, PhD thesis, Swinburne University of Technology, Melbourne, Victoria
Han J. L. et al., 2021, Res. Astron. Astrophys., 21, 107
Han J. L. et al., 2025, Res. Astron. Astrophys., 25, 014001
Hankins T. H., 1996, in Johnston S., Walker M. A., Bailes M., eds, ASP Conf. Ser. Vol. 105, Proc. IAU Colloq. 160, Pulsars: Problems and Progress. Astron. Soc. Pac., San Francisco, p. 197
Hessels J. W. T., Ransom S. M., Kaspi V. M., Roberts M. S. E., Champion D. J., Stappers B. W., 2008, in Bassa C., Wang Z., Cumming A., Kaspi V. M., eds, AIP Conf. Proc. Vol. 983, 40 Years of Pulsars: Millisecond Pulsars, Magnetars and More. Am. Inst. Phys., New York, p. 613
Hobbs G. B., Edwards R. T., Manchester R. N., 2006, MNRAS, 369, 655
Hurley-Walker N. et al., 2022, Nature, 601, 526
Hurley-Walker N. et al., 2023, Nature, 619, 487
Hurley-Walker N. et al., 2024, ApJ, 976, L21
Hyman S. D., Lazio T. J. W., Kassim N. E., Ray P. S., Markwardt C. B., Yusef-Zadeh F., 2005, Nature, 434, 50
Jankowski F. et al., 2023, MNRAS, 524, 4275
Johnston S., Karastergiou A., 2019, MNRAS, 485, 640
Jonas J., MeerKAT Team, 2018, PoS, MeerKAT2016, 001
Kaspi V. M., Beloborodov A. M., 2017, ARA&A, 55, 261
Keane E. F., McLaughlin M. A., 2011, Bull. Astron. Soc. India, 39, 333
Keane E. F. et al., 2018, MNRAS, 473, 116
Keith M. J. et al., 2010, MNRAS, 409, 619
Kramer M., Liu K., Desvignes G., Karuppusamy R., Stappers B. W., 2024, Nat. Astron., 8, 230
Law C. J. et al., 2018, ApJS, 236, 8
Lee Y. W. J. et al., 2025, Nat. Astron., 9, 393
Lehmensiek R., Theron I. P., 2012, in 2012 International Conference on Electromagnetics in Advanced Applications. IEEE, Piscataway, NJ, p. 321
Lehmensiek R., Theron I. P., 2014, in The 8th European Conference on Antennas and Propagation (EuCAP 2014). IEEE, Piscataway, NJ, p. 880
Liu X. et al., 2025, ApJ, 988, 175
Lorimer D. R., McLaughlin M. A., Bailes M., 2024, Ap&SS, 369, 59
Lu J. et al., 2019, Sci. China Phys. Mech. Astron., 62, 959503

Lyne A. G., McLaughlin M. A., Keane E. F., Kramer M., Espinoza C. M., Stappers B. W., Palliyaguru N. T., Miller J., 2009, MNRAS, 400, 1439
McConnell D. et al., 2020, Publ. Astron. Soc. Aust., 37, e048
Maciesiak K., Gil J., Melikidze G., 2012, MNRAS, 424, 1762
McLaughlin M. A., Cordes J. M., 2003, ApJ, 596, 982
McLaughlin M. A. et al., 2006, Nature, 439, 817
McLaughlin M. A. et al., 2009, MNRAS, 400, 1431
Macquart J.-P. et al., 2010, Publ. Astron. Soc. Aust., 27, 272
McSweeney S. J. et al., 2025, MNRAS, 542, 203
Majid W. A. et al., 2021, ApJ, 919, L6
Manchester R. N. et al., 2001, MNRAS, 328, 17
Mauch T. et al., 2020, ApJ, 888, 61
Mckinven R. et al., 2025, Nature, 637, 43
Mcsweeney S. J., Moseley J., Hurley-Walker N., Grover G., Horváth C., Galvin T. J., Meyers B. W., Tan C. M., 2025, ApJ, 981, 143
Men Y., Barr E., 2024, A&A, 683, A183
Mereghetti S., Pons J. A., Melatos A., 2015, Space Sci. Rev., 191, 315
Meyers B. W. et al., 2018, ApJ, 869, 134
Meyers B. W. et al., 2019, Publ. Astron. Soc. Aust., 36, e034
Mitra D., Arjunwadkar M., Rankin J. M., 2015, ApJ, 806, 236
Morello V. et al., 2020a, MNRAS, 493, 1165
Morello V., Barr E. D., Stappers B. W., Keane E. F., Lyne A. G., 2020b, MNRAS, 497, 4654
Morello V., Rajwade K. M., Stappers B. W., 2022, MNRAS, 510, 1393
Offringa A. R. et al., 2014, MNRAS, 444, 606
Padmanabh P. V. et al., 2023, MNRAS, 524, 1291
Panda U., Bhattacharyya S., Dudeja C., Kudale S., Roy J., 2024, Astron. Telegram, 16494, 1
Pastor-Marazuela I. et al., 2023, A&A, 678, A149
Pastor-Marazuela I. et al., 2025, preprint (arXiv:2507.05982)
Patel C. et al., 2018, ApJ, 869, 181
Platts E., Weltman A., Walters A., Tendulkar S. P., Gordin J. E. B., Kandhai S., 2019, Phys. Rep., 821, 1
Posselt B. et al., 2021, MNRAS, 508, 4249
Price D. C., Flynn C., Deller A., 2021, Publ. Astron. Soc. Aust., 38, e038
Rajwade K. M., van Leeuwen J., 2024, Universe, 10, 158
Rajwade K. M. et al., 2022, MNRAS, 514, 1961
Rajwade K. M. et al., 2024, MNRAS, 532, 3881
Ransom S. M., Eikenberry S. S., Middleditch J., 2002, AJ, 124, 1788
Rea N. et al., 2009, ApJ, 703, L41
Sanidas S., Caleb M., Driessen L., Morello V., Rajwade K., Stappers B. W., 2018, in Weltevrede P., Perera B. B. P., Preston L. L., Sanidas S., eds, Proc. IAU Symp. Vol. 337, Pulsar Astrophysics the Next Fifty Years. Cambridge Univ. Press, Cambridge, p. 406
Sengar R. et al., 2023, MNRAS, 522, 1071
Singh S., Roy J., Panda U., Bhattacharyya B., Morello V., Stappers B. W., Ray P. S., McLaughlin M. A., 2022, ApJ, 934, 138
Singh S., Roy J., Sharma S. S., Bhattacharyya B., Kudale S., 2023, ApJ, 954, 160
Skrzypczak A., Basu R., Mitra D., Melikidze G. I., Maciesiak K., Koralewska O., Filothodoros A., 2018, ApJ, 854, 162
Staelin D. H., 1969, IEEE Proc., 57, 724
Stappers B., 2018, PoS, MeerKAT2016, 010
Stappers B. W., Keane E. F., Kramer M., Possenti A., Stairs I. H., 2018, Philos. Trans. R. Soc. A, 376, 20170293
Surnis M. P. et al., 2023, MNRAS, 526, L143
Tan C. M. et al., 2018, ApJ, 866, 54
Tian J. et al., 2024, MNRAS, 533, 3174
Turner J. D. et al., 2025, MNRAS, 537, 1070
van Heerden E., Karastergiou A., Roberts S. J., 2017, MNRAS, 467, 1661
Venkatraman Krishnan V. et al., 2020, MNRAS, 492, 4752
Vink J., 2020, Physics and Evolution of Supernova Remnants. Springer, Cham, Switzerland
Wang Y. et al., 2025, ApJ, 982, L53
Wang Z. et al., 2025a, Nature, 642, 583
Wang Z. et al., 2025b, Publ. Astron. Soc. Aust., 42, e005
Weltevrede P., 2016, A&A, 590, A109
Wenger M. et al., 2000, A&AS, 143, 9
Wielebinski R., Junkes N., Grahl B. H., 2011, J. Astron. Hist. Herit., 14, 3
Yamasaki S., Totani T., 2020, ApJ, 888, 105
Yao J. M., Manchester R. N., Wang N., 2017, ApJ, 835, 29
Zhang B., 2023, Rev. Mod. Phys., 95, 035005
Zhang J. et al., 2024, Astron. Telegram, 16433, 1
Zhou P., Vink J., Li G., Domček V., 2018, ApJ, 865, L6
Zhou D. J. et al., 2023, Res. Astron. Astrophys., 23, 104001

APPENDIX A: IMAGES

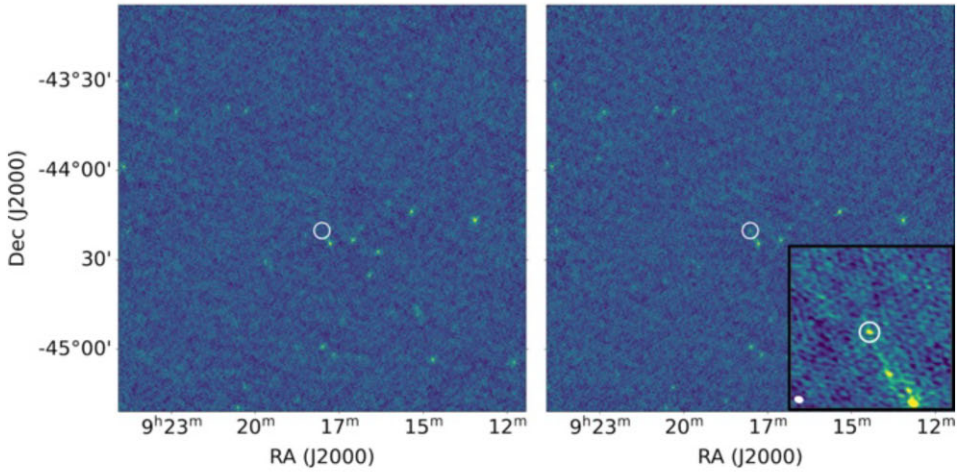

(a) MTP0055

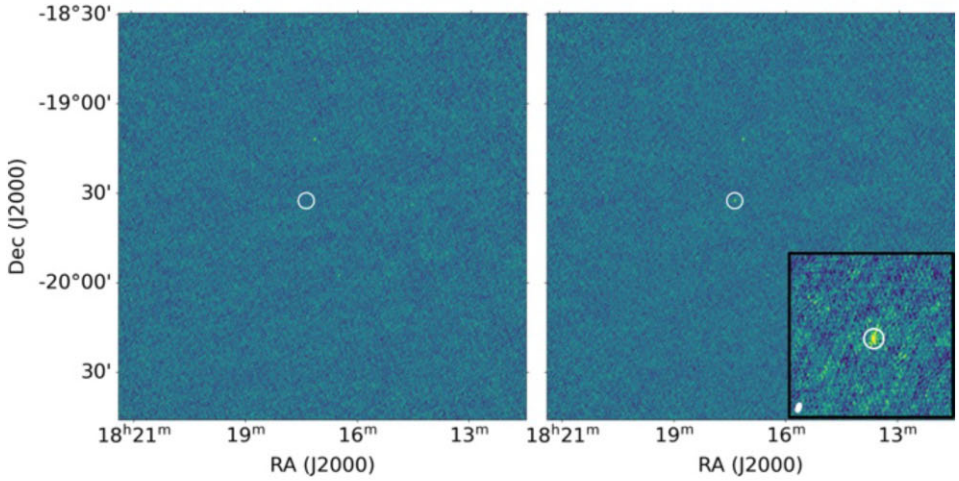

(b) MTP0063

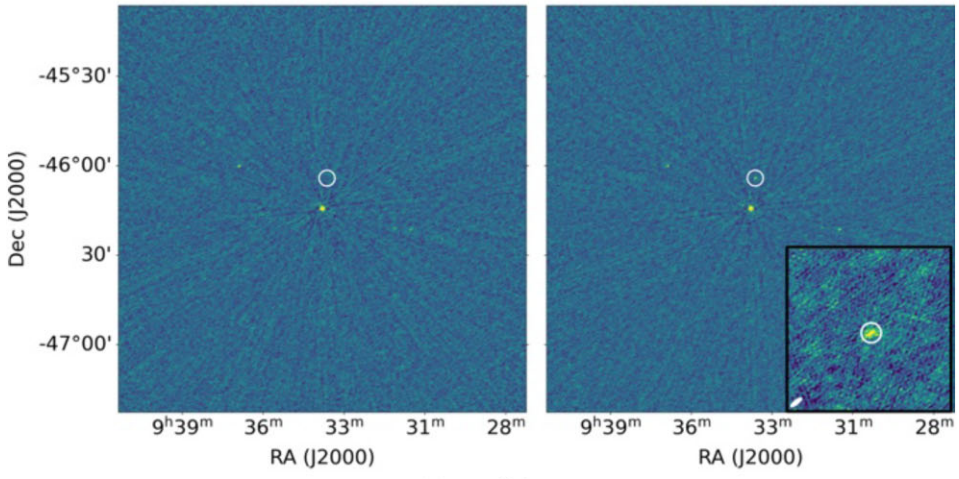

(c) MTP0067

Figure A1. Images of the nine MTP sources that triggered the transient buffer to save voltage data (see Section 2.1.3). For each source, we show the image integrated over the duration of the pulse (right) and before the pulse detection (left). The magenta circle in the on-pulse image marks the transient source identified at the pulse detection, and the inset at the bottom right corner is a zoomed-in view of the source. The synthesized beam is shown at the bottom left corner of the inset.

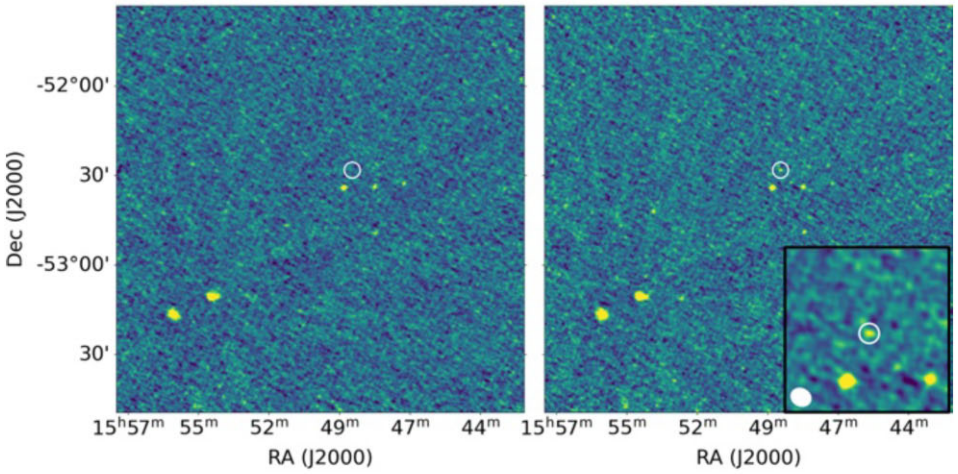

(a) MTP0069

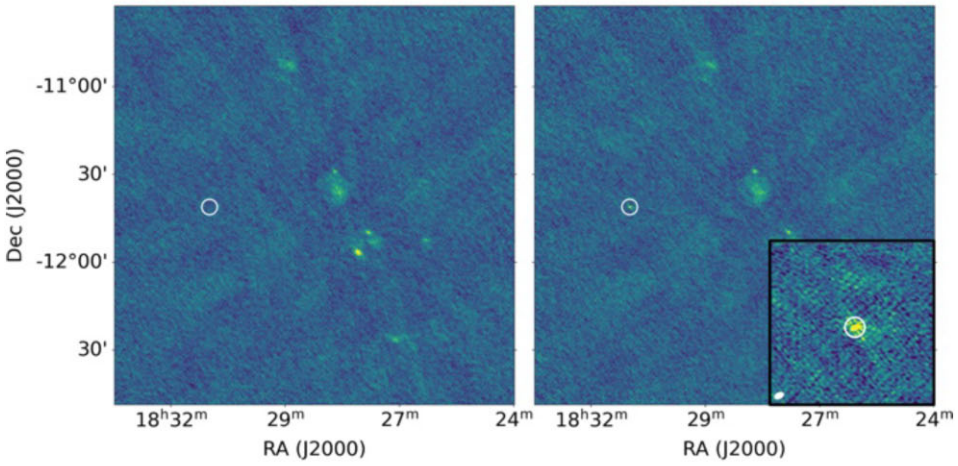

(b) MTP0072

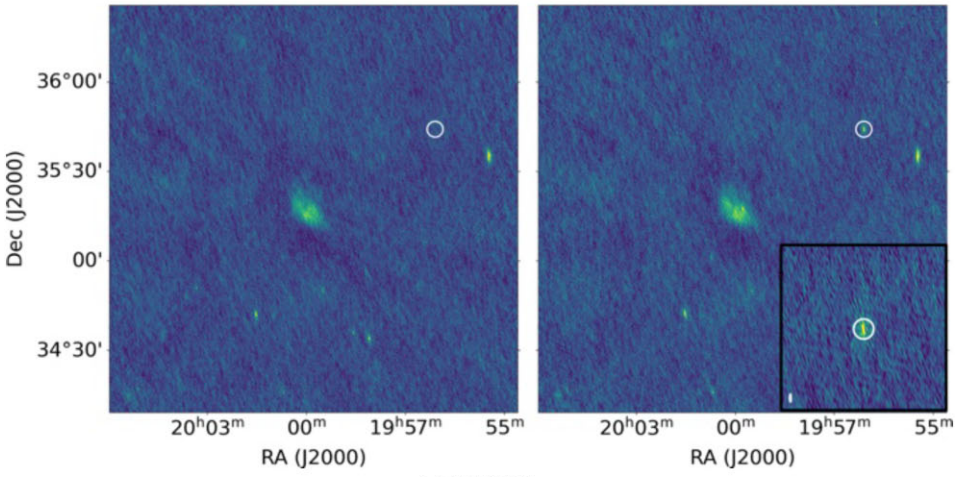

(c) MTP0074

Figure A1. (*Continued.*)

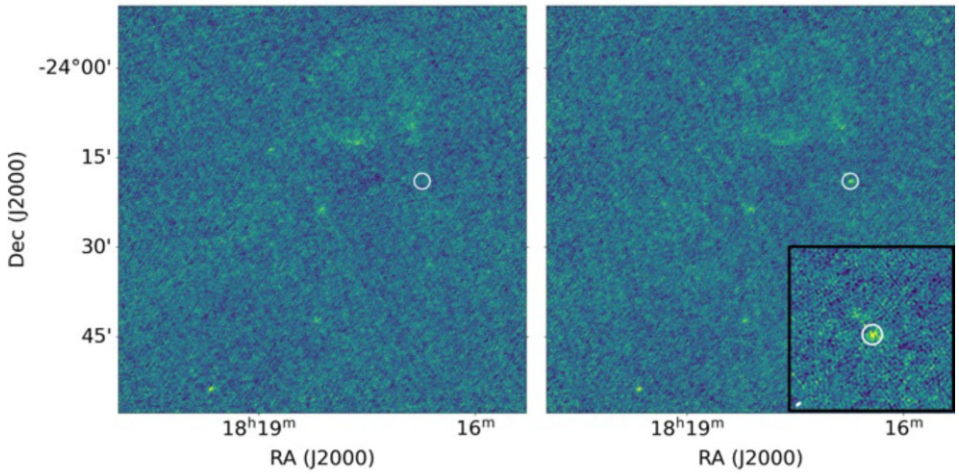

(a) MTP0079

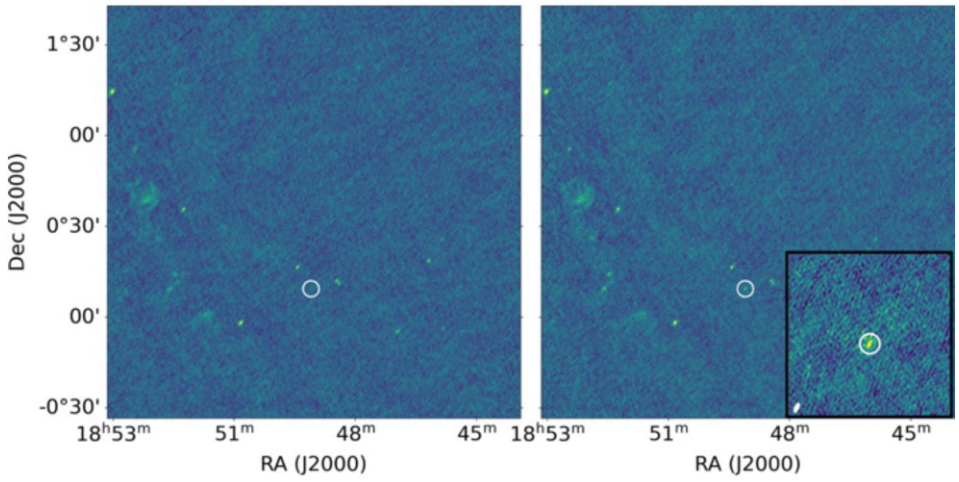

(b) MTP0080

Figure A1. (*Continued*.)

This paper has been typeset from a TEX/LATEX file prepared by the author.